# Tungsten–Carbon, Carbon–Hydrogen, and Carbon–Carbon Bond Activation in the Chemistry of 1,2-$W_2R_2(OR')_4$($W \equiv W$) Complexes. 2. Metal–Carbon Bond Homolysis and Competitive Alkane and Dihydrogen Eliminations in Double $\alpha$-Hydrogen Activation Processes

Malcolm H. Chisholm,* Bryan W. Eichhorn, and John C. Huffman

*Department of Chemistry and Molecular Structure Center, Indiana University, Bloomington, Indiana 47405*

*Received January 28, 1988*

Thermolysis of bis(alkyne) adducts of formula $W_2(CH_2R)_2(MeCCMe)_2(O\text{-}i\text{-}Pr)_4$ (**1a**) (where R = Ph, $SiMe_3$, and *t*-Bu) in hydrocarbon solutions produces $HW_2(\mu\text{-}CR)(\mu\text{-}C_4Me_4)(O\text{-}i\text{-}Pr)_4$ ((**2**)H) and $(RCH_2)W_2(\mu\text{-}CR)(\mu\text{-}C_4Me_4)(O\text{-}i\text{-}Pr)_4$ ((**2**)R) by competitive reaction pathways. The formation of compounds (**2**)H and (**2**)R requires coupling of terminal alkyne ligands and double $\alpha$-hydrogen abstractions of one alkyl ligand. One equivalent of $RCH_3$ or $H_2$ is produced for each mole of (**2**)H or (**2**)R formed, respectively. In all cases, (**2**)H is the major reaction product. In the solid state, a thermal crystal-to-powder decrepitation of (**1a**)($SiMe_3$) occurs to produce a 2:1 mixture of (**2**)H($SiMe_3$) and (**2**)R($SiMe_3$) with $t_{1/2} \approx 100$ days at room temperature. Compounds of formula $W_2(CH_2R)_2(R'CCR'')_2(O\text{-}i\text{-}Pr)_4$ (where R = *t*-Bu, R′ = Me, R″ = Et; R = $SiMe_3$ or Ph, R′ = Et, R″ = Me or Et) react thermally to form a mixture of as yet unidentified organometallic products. No analogues of **2** with $MC_4$ rings bearing Et substituents were unequivocally identified. The benzyl derivatives of **1** (where R = Ph) react photochemically at low temperatures (10 °C) to form $W_2(\mu\text{-}C_2R'_2)_2(O\text{-}i\text{-}Pr)_4$ (**3a**, R′ = Me; **3c**, R′ = Et) and bibenzyl as the major reaction products. Mechanistic studies of the formation of compounds **3** are indicative of metal–carbon bond homolysis. Compounds **2** were characterized by $^1H$ NMR, $^{13}C$ NMR, and IR spectroscopic studies and elemental analysis. Compounds (**2**)H(Ph) and (**2**)R($SiMe_3$) were structurally characterized by single-crystal X-ray diffraction. The two molecules are virtually isostructural with symmetrical alkylidyne bridges [W–C = 1.96 (2) Å (average)] and single W–W bonds [W–W = 2.77 (2) Å (average)]. The hydride ligand of (**2**)H(Ph) was not located in the crystallographic study but was assigned the position trans to the $\eta^4$-$C_4Me_4$ ring based on NOE difference NMR experiments. The low-temperature limiting NMR spectra for **2** are consistent with the solid-state structures but at ambient temperatures and above, a fluxional process is observed involving inversion of configuration at one metal center. Mechanistic studies revealed intramolecular first-order reactions for the thermolyses of **1** with the rates of reaction (and rate constants) following the series for the three alkyl ligands $k_{t\text{-}Bu} > k_{SiMe_3} > k_{Ph}$ and the alkyne ligands substituents (R′ = R″) $k_{Me} \gg k_{Et}$. A small kinetic isotope effect, $k_H/k_D = 1.4$, was observed when $W_2(CD_2Ph)_2(MeCCMe)_2(O\text{-}i\text{-}Pr)_4$ was employed. The activation parameters for (**1a**)(Ph) and (**1a**)($SiMe_3$) are $\Delta S^\ddagger = -9$ eu, $\Delta H^\ddagger = 21$ kcal mol$^{-1}$ and $\Delta S^\ddagger = -9$ eu, $\Delta H^\ddagger = 23$ kcal mol$^{-1}$, respectively, indicating that the differences in rates are enthalpic in origin. The data are most consistent with a rate-determining alkyne-coupling step that is followed by the C–H activation processes. Comparisons of these reactions with mononuclear orthometalation and $\alpha$-hydrogen abstraction reactions are presented. Crystal data for $W_2(H)(\mu\text{-}CPh)(\mu\text{-}C_4Me_4)(O\text{-}i\text{-}Pr)_4$ at −159 °C: $a = 9.183$ (3) Å, $b = 15.606$ (6) Å, $c = 19.977$ (9) Å, $Z = 4$, $d_{calcd} = 1.862$ g cm$^{-3}$, space group $P2_12_12_1$; for $W_2(CH_2SiMe_3)(\mu\text{-}CSiMe_3)(\mu\text{-}C_4Me_4)(O\text{-}i\text{-}Pr)_4$ at −155 °C: $a = 11.906$ (4) Å, $b = 15.633$ (5) Å, $c = 9.584$ (3) Å, $\alpha = 90.47$ (2)°, $\beta = 99.49$ (2)°, $\gamma = 91.27$ (2)°, $d_{calcd} = 1.738$ g cm$^{-3}$, space group $P\bar{1}$.

## Introduction

In the preceding paper,[1] we described the synthesis and characterization of a series of dialkyl, bis(alkyne) compounds of formula $W_2(CH_2R)_2(R'CCR'')_2(O\text{-}i\text{-}Pr)_4$ (**1**). These compounds react thermally and photochemically in solution by a variety of pathways involving C–H and W–C activations of the hydrocarbyl ligands ($CH_2R$). To systematically investigate the modes of hydrocarbyl degradation, we have independently studied $\alpha$-C–H abstraction in the absence of $\beta$-C–H activation by employing alkyl ligands that contain no $\beta$-hydrogens, namely, where $CH_2R$ = $CH_2Ph$, $CH_2SiMe_3$, and $CH_2$-*t*-Bu. During these investigations, we discovered a remarkable reaction involving the abstraction of two $\alpha$-hydrogens that are ultimately expelled as molecular $H_2$. In the following paper,[2] we describe the $\beta$-hydrogen elimination reactions of **1** and reactions in which $\alpha$- and $\beta$-hydrogen activations are competitive. We report here the synthetic and mechanistic details on the thermal formations of alkylidyne hydride and alkylidyne alkyl compounds of formula $XW_2(\mu\text{-}CR)(\mu\text{-}C_4Me_4)(O\text{-}i\text{-}Pr)_4$, where X = hydride or alkyl, derived from double $\alpha$-hydrogen abstractions of coordinated alkyl ligands. The photochemical decompositions of compounds **1** to form bis(alkyne)-bridged compounds $W_2(\mu\text{-}C_2R'_2)_2(O\text{-}i\text{-}Pr)_4$ from M–C bond homolysis are also discussed. The spectroscopic and structural properties of these compounds are presented. A preliminary account of some of this work has appeared.[3]

## Abbreviations for Compounds

The compounds of formula $W_2(CH_2R)_2(R'CCR'')_2(O\text{-}i\text{-}Pr)_4$ (**1**) are referred to as **1a** when R′ = R″ = Me, **1b** when R′ = Et and R″ = Me, and **1c** when R′ = R″ = Et. The thermal and photochemical decomposition products of **1a** having the formula $XW_2(\mu\text{-}CR)(\mu\text{-}C_4Me_4)(O\text{-}i\text{-}Pr)_4$ where X = H or $CH_2R$ are referred to as (**2**)R when X = $CH_2R$ or (**2**)H when X = H. When a unique compound is specified, the identity of R will immediately follow the

(1) Chisholm, M. H.; Eichhorn, B. W.; Folting, K.; Huffman, J. C. *Organometallics*, first of three papers in this issue.
(2) Chisholm, M. H.; Eichhorn, B. W.; Huffman, J. C. *Organometallics*, third of three papers in this issue.
(3) Chisholm, M. H.; Eichhorn, B. W.; Huffman, J. C. *J. Chem. Soc., Chem. Commun.* **1985**, 861.

0276-7333/89/2308-0067$01.50/0 © 1989 American Chemical Society

**Scheme I**

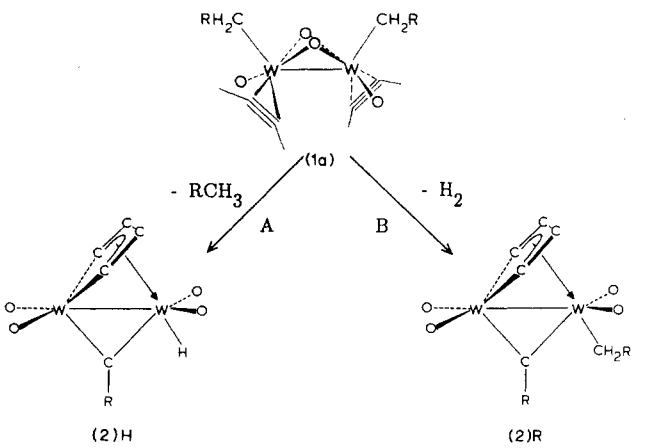


O = O-*i*-Pr

compound number. For example, the compounds $(Me_3SiCH_2)W_2(\mu\text{-}CSiMe_3)(\mu\text{-}C_4Me_4)(O\text{-}i\text{-}Pr)_4$ and $W_2(CH_2Ph)_2(MeCCMe)_2(O\text{-}i\text{-}Pr)_4$ are referred to (2)R($SiMe_3$) and (**1a**)(Ph), respectively. Statements and discussions concerning compounds **2** are applicable to both (2)H and (2)R unless specifically noted. Compounds $W_2(\mu\text{-}C_2Me_2)_2(O\text{-}i\text{-}Pr)_4$ and $W_2(\mu\text{-}C_2Et_2)_2(O\text{-}i\text{-}Pr)_4$ are referred to as **3a** and **3c**, respectively.

## Synthesis and Reactivity

**Thermolysis of 1,2-$W_2(CH_2R)_2(MeCCMe)_2(O\text{-}i\text{-}Pr)_4$ Compounds.** Compounds of formula 1,2-$W_2(CH_2R)_2(MeCCMe)_2(O\text{-}i\text{-}Pr)_4$ (**1a**, where R = Ph, $SiMe_3$) thermally react in hydrocarbon and ethereal solutions by competitive $\alpha$-hydrogen activation pathways according to Scheme I. The dominant mode of reaction (Scheme I, path A) involves alkane elimination to generate alkyne-coupled, alkylidyne hydride complexes of formula $HW_2(\mu\text{-}CR)(\mu\text{-}C_4Me_4)(O\text{-}i\text{-}Pr)_4$ ((2)H). The secondary mode of reaction (Scheme I, path B) liberates molecular $H_2$ and produces alkyne-coupled alkylidyne alkyl complexes of formula $(RCH_2)W_2(\mu\text{-}CR)(\mu\text{-}C_4Me_4)(O\text{-}i\text{-}Pr)_4$ ((2)R). The two reactions are related in that both involve double $\alpha$-hydrogen activations of one alkyl ligand and coupling of terminal alkyne ligands to form $MC_4$ metallacyclopentadiene rings. Path A requires a transfer of one $\alpha$-hydrogen to a neighboring alkyl ligand and one to the metal center producing an alkylidyne hydride fragment and 1 equiv of alkane. Labeling studies show that the $\alpha$-H atom transfers are nonradical and intramolecular and will be discussed in detail later. Path B involves abstraction and expulsion of two $\alpha$-hydrogens of one alkyl ligand to generate an alkylidyne fragment and 1 equiv of $H_2$. In an analogous reaction 1,2-$W_2(CH_2\text{-}t\text{-}Bu)_2(O\text{-}i\text{-}Pr)_4$ reacts with 2 equiv of 2-butyne to produce $HW_2(\mu\text{-}C\text{-}t\text{-}Bu)(\mu\text{-}C_4Me_4)(O\text{-}i\text{-}Pr)_4$, (2)H(*t*-Bu), and 1 equiv of $CMe_4$ according to eq 1. When

$$W_2(CH_2\text{-}t\text{-}Bu)_2(O\text{-}i\text{-}Pr)_4 + 2\ MeC{\equiv}CMe \rightarrow HW_2(\mu\text{-}C\text{-}t\text{-}Bu)(\mu\text{-}C_4Me_4)(O\text{-}i\text{-}Pr)_4 + CMe_4 \quad (1)$$
$$\text{(2)H}(t\text{-Bu})$$

less than 2 equiv of 2-butyne are used in reaction 1, mixtures of (2)H(*t*-Bu) and $W_2(CH_2\text{-}t\text{-}Bu)_2(O\text{-}i\text{-}Pr)_4$ are recovered. Although compound (**1a**)(*t*-Bu) could not be isolated or detected spectroscopically at −78 °C, it is the most likely intermediate in the formation of (2)H(*t*-Bu).

Thermolysis of compound (**1a**)($SiMe_3$) in a Pyrex NMR tube in benzene-$d_6$ or toluene-$d_8$ reproducibly yields 90:10 mixtures of (2)H($SiMe_3$) to (2)R($SiMe_3$) regardless of temperature, concentration, NMR tube condition or age, or exposure to low intensity light. In a Schlenk flask, however, thermolyses of (**1a**)($SiMe_3$) in a variety of solvents produce 45:55 mixtures of (2)H($SiMe_3$) to (2)R($SiMe_3$), respectively, and are also insensitive to concentration or exposure to low intensity light. Slight variances were observed from flask to flask with product ratios [(2)H($SiMe_3$):(2)R($SiMe_3$)] ranging from 40:60 to 55:45, but the ratio never approached the 90:10 distribution that was observed in an NMR tube. Rigorous and repetitive experiments were conducted to probe the effect of impurities such as *i*-PrOH, benzophenone, $H_2$, $SiMe_4$, or trace amounts of $H^+$ or $OH^-$ adsorbed onto the glass surface (see Experimental Section, Table XI). None of these factors had any significant effect on the product distributions. Solvent effects observed using benzene, benzene-$d_6$, toluene, toluene-$d_8$, pentane, hexane, or $Et_2O$ were essentially negligible when the reactions were carried out in NMR tubes. The product distributions in benzene and benzene-$d_6$ were identical within experimental error. Experiments conducted in new glass vials in a drybox indicated that glass surface area may have some effect on product distribution. The control experiment (regular vial) produced a (2)H($SiMe_3$):(2)R($SiMe_3$) ratio of 67:33 but when finely ground Pyrex glass was added in a concurrent experiment, the ratio was shifted to 50:50 (average) under otherwise identical conditions. Similar experiments in which finely ground Pyrex glass was loaded into NMR tubes also shifted the product ratios to 66:34 (average), but internally consistent values between reactions conducted in Schlenk flasks and NMR tubes were never attained. The factors affecting these puzzling product distributions remain to be established.

In the solid state, $W_2(CH_2SiMe_3)_2(MeCCMe)_2(O\text{-}i\text{-}Pr)_4$ ((**1a**)($SiMe_3$)) also thermally decomposes according to Scheme I to form a 2:1 mixture of (2)H($SiMe_3$) and (2)R($SiMe_3$). The half-life ($t_{1/2}$) for this process is ca. 100 days at room temperature and is insensitive to light. No oils or liquids were observed during the crystal-to-powder decrepitation. Compound (**1a**)(Ph), however, is stable in the solid state for more than 1 year at ambient temperatures under $N_2$ atmospheres.

Compounds **2** were isolated by either fractional crystallization [(2)H(Ph); (2)R($SiMe_3$)] or sublimation [(2)H(*t*-Bu); (2)H($SiMe_3$)]. Compound (2)R(Ph) was only observed in small quantities by $^1H$ NMR spectroscopy, and no analogue of (2)R(*t*-Bu) has been isolated or detected spectroscopically. The isolated species were characterized by $^1H$ NMR, $^{13}C\{^1H\}$ NMR, and IR spectroscopic studies elemental analysis [except (2)R($SiMe_3$)] and a representative of each structural type has been characterized by X-ray crystallography. The alkane and molecular $H_2$ byproducts were identified by $^1H$ NMR and mass spectroscopy, respectively. Compounds **2** are pale yellow to orange in color and are moderately air- and moisture-sensitive in solution and in the solid state. The elemental analyses for the three hydrido compounds (2)H(R = Ph, $SiMe_3$, or *t*-Bu) all registered low in carbon content by one carbon atom per molecule (see Experimental Section). The "missing" carbon atom is most likely the alkylidyne $W_2(\mu\text{-}CR)$ carbon that presumably forms undetectable tungsten carbide during combustion.[4] Compounds **2** are inert toward additional equivalents of ethyne, 2-butyne, and molecular $H_2$ (500 psi). The hydride ligands of (2)H do not react with weak acids or bases (*i*-PrOH and LiO-*i*-Pr, respectively) and do not undergo H/D exchange with *i*-PrO*D* even in the presence of LiO-*i*-Pr. The hydride resonances of (2)H are not exchange broadened in the $^1H$

(4) Blau, R. J.; Chisholm, M. H.; Folting, K.; Huffman, J. C.; Wang, R. J. *J. Chem. Soc., Chem. Commun.* **1985**, 1466.

**Scheme II**

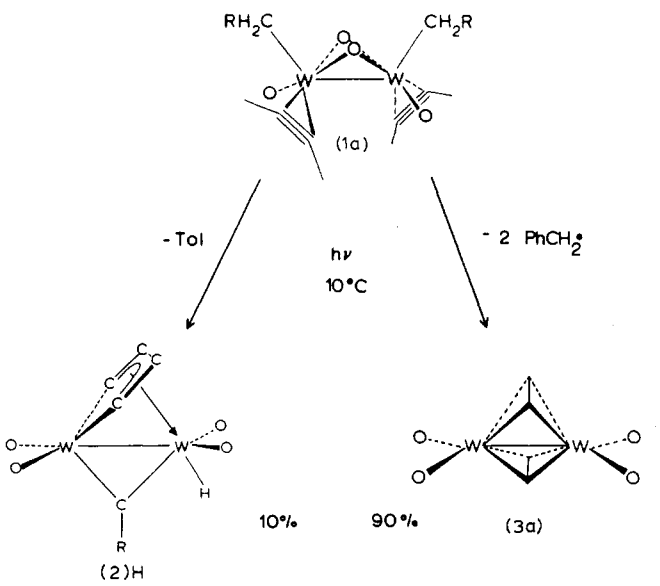


O = O-*i*-Pr; R = Ph

NMR spectrum when *i*-PrOH is present. Compounds **2**(R) and **2**(H) *cannot* be interconverted by either adding $RCH_3$ to **2**(H) or, as just mentioned, by adding $H_2$ to **2**(R).

**Photolysis of 1,2-$W_2(CH_2R)_2(MeCCMe)_2(O\text{-}i\text{-}Pr)_4$ Compounds.** The photochemical reactions of compounds **1a** are more dependent upon the nature of the alkyl ligand than the thermal reactions just described. Photolysis of (**1a**)(Ph) in $C_6D_6$ in a Pyrex NMR tube yields (**2**)H(Ph) and the bis(alkyne)-bridged compound $W_2(\mu\text{-}C_2Me_2)_2(O\text{-}i\text{-}Pr)_4$ (**3a**) in a 1:9 ratio according to Scheme II. Formally, path A of Scheme II is the same as path A in Scheme I, although mechanistically, tungsten–carbon bond homolysis may be operative in the former but not in the latter. Path C of Scheme II involves elimination of 2 equiv of benzyl radicals to produce the formally reduced compound **3a**. In the absence of good hydrogen atom donors (i.e. 1,4-cyclohexadiene), the organic byproducts favor bibenzyl over toluene by a ca. 4:1 ratio. In the presence of 1,4-cyclohexadiene (ca. 6 equiv), the relative yields of (**2**)H(Ph) and **3a** are unchanged, but the bibenzyl to toluene ratio is lowered to ca. 2:1 with the concomitant formation of $C_6H_6$. In both cases, small quantities (≤10%) of other unidentified products were produced.

The photochemical decomposition of (**1a**)($SiMe_3$) is quite different than that of (**1a**)(Ph). Most notably, photolysis of (**1a**)($SiMe_3$) in $C_6D_6$ liberates $SiMe_4$ but does not produce any detectable quantities of (**2**)H($SiMe_3$), (**2**)R($SiMe_3$), or **3a**. In the presence of 1,4-cyclohexadiene (ca. 6 equiv), the rate of formation of $SiMe_4$ is approximately doubled, but no other organic or organometallic products have yet been identified. Furthermore, (**1a**)(Ph) reacts four times faster than (**1a**)($SiMe_3$) under identical conditions.

These data are consistent with photochemically induced, metal–carbon bond homolysis. The formation of bibenzyl and the increased formation of alkane ($SiMe_4$ or toluene) in the presence of 1,4-cyclohexadiene is indicative of free or caged alkyl radicals being generated in solution. Thermal, nonradical decompositions of (**1a**)(Ph) liberate toluene as the only organic byproduct, even at +80 °C, and do not produce detectable quantities of **3a**. The marked differences in the photodecompositions of (**1a**)(Ph) and (**1a**)($SiMe_3$) may be due to one of the following. (1) The proportion of alkyl radicals that escape from the radical cage is greater for $PhCH_2^\bullet$ versus $Me_3SiCH_2^\bullet$ due to the greater relative stability of the benzyl radical. The unstable $Me_3SiCH_2^\bullet$ radical would either recombine with the metal-centered radical, in a nonproductive fashion, or abstract the nearest hydrogen leading to the observed random (i.e. nonselective) decomposition of the compound. (2) The benzyl ligand could be acting as an intramolecular photosensitizer in (**1a**)(Ph) facilitating rapid photochemical decomposition relative to (**1a**)($SiMe_3$).

The electronic absorption spectral data for compounds **1** are given in the preceding paper.[1] Although definitive assignments were not possible, the medium intensity bands ($\epsilon \sim 2600$) between 400 and 500 nm clearly show alkyl group dependencies. This behavior suggests that contributions from W–C $\sigma$ or $\sigma^*$ orbitals may be involved in these transitions. The tail of the $\pi \rightarrow \pi^*$ transition of the phenyl ring for (**1a**)(Ph) at 268 nm is also photochemically accessible in a Pyrex NMR tube.[5]

The bis(alkyne)-bridged compound $W_2(\mu\text{-}C_2Me_2)_2(O\text{-}i\text{-}Pr)_4$ (**3a**) can be isolated from photolyzed hexane solutions of (**1a**)(Ph) as a brown crystalline solid but is more conveniently prepared by other methods.[2] In solution, **3a** adopts the structure depicted in Scheme II and is very air- and moisture-sensitive in both solution and the crystalline state. It has been characterized by $^1H$ NMR, $^{13}C\{^1H\}$ NMR, and IR spectroscopic techniques, elemental analysis, and X-ray crystallography. The solid-state structure and spectroscopic properties of **3a** will be discussed in the following paper of this issue.[2]

**Thermolysis of 1,2-$W_2(CH_2R)_2(R'CCR'')_2(O\text{-}i\text{-}Pr)_4$ Compounds.** Compounds of formula 1,2-$W_2(CH_2R)_2(R'CCR'')_2(O\text{-}i\text{-}Pr)_4$ (**1b** and **1c**, where R = $SiMe_3$ or Ph, R′ = Et, and R″ = Me or Et) are much more thermally robust in hydrocarbon solutions than **1a** where R′ = R″ = Me. Relatively high temperatures (ca. 70 °C) and long reaction times ($t_\infty$ = 2–5 days) are required to complete the decompositions of the former. Thermolysis of compounds **1c** in the dark promotes intramolecular alkane elimination (≥1 equiv) an alkyne coupling to give mixtures of as yet unidentified products. No analogues of **2** (where R = $SiMe_3$ or Ph) with $MC_4$ metallacycles bearing Et substituents have been unequivocally identified thus far. The decompositions are first-order in **1c** and will be discussed later.

1,2-$W_2(CH_2\text{-}t\text{-}Bu)_2(O\text{-}i\text{-}Pr)_4$ reacts with MeC≡CEt (≥2 equiv) to give a mixture of products, none of which have been unequivocally identified. However, $^1H$ NMR spectra of the crude reaction mixtures reveal three equal intensity hydride signals at 19.8, 19.9, and 20.0 ppm with tungsten satellites characteristic of compounds of type (**2**)H($\delta$(W–H) ca. 20 ppm downfield of $SiMe_4$ with $^1J_{^{183}W\text{-}^1H} \approx 125$ Hz). The data are consistent with the formation of three isomers of $HW_2(\mu\text{-}C\text{-}t\text{-}Bu)(\mu\text{-}C_4Me_2Et_2)(O\text{-}i\text{-}Pr)_4$ ((**2′**)H(*t*-Bu)) as would be expected from the three possible coupling modes of the MeCCEt ligands. The three possible isomers of the $MC_4$ metallacycles, I–III, are shown. A fourth resonance

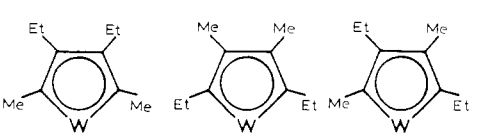


I II III

of much lower relative intensity is consistently observed at 20.1 ppm and is broader than the other three. This resonance could represent the fourth possible isomer of (**2′**)H(*t*-Bu) in which the two Me and two Et substituents are mutually cis on the $MC_4$ ring. The mixture of isomers

(5) Pyrex glass does not transmit light below 290 nm.

**Table I. Selected Bond Distances (Å) and Angles (deg) for $HW_2(\mu\text{-}CPh)(\mu\text{-}C_4Me_4)(O\text{-}i\text{-}Pr)_4$**

| Bond Distances | | | |
|---|---|---|---|
| W(1)–W(2) | 2.7554 (16) | W(2)–O(26) | 1.870 (14) |
| W(1)–O(18) | 1.891 (19) | W(2)–O(30) | 1.900 (18) |
| W(1)–O(22) | 1.925 (16) | W(2)–C(4) | 2.102 (22) |
| W(1)–C(4) | 2.391 (22) | W(2)–C(7) | 2.081 (25) |
| W(1)–C(5) | 2.478 (22) | W(2)–C(11) | 1.950 (23) |
| W(1)–C(6) | 2.468 (21) | C(4)–C(5) | 1.42 (3) |
| W(1)–C(7) | 2.430 (21) | C(5)–C(6) | 1.44 (4) |
| W(1)–C(11) | 1.975 (17) | C(6)–C(7) | 1.46 (4) |
| | | C(11)–C(12) | 1.52 (4) |

| Bond Angles | | | |
|---|---|---|---|
| W(1)–C(11)–W(2) | 89.2 (11) | W(1)–O(18)–C(19) | 130.6 (15) |
| W(1)–C(11)–C(12) | 140.0 (16) | W(1)–O(22)–C(23) | 133.8 (17) |
| W(2)–C(11)–C(12) | 130.7 (17) | W(2)–O(26)–C(27) | 155.0 (14) |
| O(18)–W(1)–O(22) | 115.0 (7) | W(2)–O(30)–C(31) | 146.8 (19) |
| O(26)–W(2)–O(30) | 97.7 (7) | | |

**Table II. Fractional Coordinates for $HW_2(\mu\text{-}CPh)(\mu\text{-}C_4Me_4)(O\text{-}i\text{-}Pr)_4$**

| atom | $10^4x$ | $10^4y$ | $10^4z$ | $10B_{iso}$, Å$^2$ |
|---|---|---|---|---|
| W(1) | 5991 (1) | 9766 (1) | 1690.7 (4) | 16 |
| W(2) | 5338 (1) | 10387 (1) | 435.1 (4) | 17 |
| C(3) | 8623 (24) | 9746 (17) | 484 (14) | 29 |
| C(4) | 7471 (26) | 10343 (16) | 815 (10) | 24 |
| C(5) | 7898 (32) | 10819 (13) | 1386 (12) | 27 |
| C(6) | 6703 (29) | 11291 (14) | 1669 (17) | 33 |
| C(7) | 5382 (32) | 11183 (13) | 1270 (13) | 26 |
| C(8) | 4028 (38) | 11627 (14) | 1535 (13) | 33 |
| C(9) | 9419 (25) | 10791 (18) | 1655 (14) | 32 |
| C(10) | 6772 (38) | 11849 (16) | 2261 (13) | 35 |
| C(11) | 4712 (30) | 9393 (15) | 951 (11) | 26 |
| C(12) | 3601 (26) | 8702 (14) | 791 (11) | 21 |
| C(13) | 3703 (24) | 7890 (14) | 1084 (14) | 24 |
| C(14) | 2710 (35) | 7289 (18) | 938 (12) | 34 |
| C(15) | 1670 (30) | 7419 (16) | 472 (15) | 32 |
| C(16) | 1623 (37) | 8220 (18) | 120 (19) | 43 |
| C(17) | 2516 (33) | 8837 (14) | 327 (15) | 35 |
| O(18) | 5049 (22) | 10177 (11) | 2469 (8) | 32 |
| C(19) | 3928 (29) | 9785 (16) | 2888 (12) | 28 |
| C(20) | 2566 (32) | 9684 (22) | 2489 (16) | 44 |
| C(21) | 3802 (37) | 10334 (22) | 3519 (14) | 47 |
| O(22) | 7696 (19) | 9079 (9) | 1853 (8) | 23 |
| C(23) | 7923 (33) | 8201 (14) | 1972 (14) | 31 |
| C(24) | 7838 (35) | 7731 (19) | 1300 (14) | 36 |
| C(25) | 9262 (35) | 8065 (19) | 2306 (16) | 42 |
| O(26) | 6084 (16) | 10042 (9) | −393 (7) | 19 |
| C(27) | 6966 (33) | 10109 (16) | −947 (13) | 34 |
| C(28) | 7640 (28) | 11025 (16) | −1026 (17) | 36 |
| C(29) | 6242 (31) | 9835 (17) | −1586 (14) | 35 |
| O(30) | 3686 (21) | 10991 (10) | 110 (9) | 30 |
| C(31) | 3124 (41) | 11781 (18) | −133 (15) | 41 |
| C(32) | 3624 (36) | 11957 (16) | −800 (16) | 40 |
| C(33) | 1478 (37) | 11734 (24) | −86 (23) | 62 |

and the presence of other products due to competitive reaction pathways have hampered product separation.

**Photolysis of 1,2-$W_2(CH_2R)_2(R'CCR'')_2(O\text{-}i\text{-}Pr)_4$ Compounds.** Photolysis of benzene-$d_6$ solutions of $W_2(CH_2Ph)_2(EtCCEt)_2(O\text{-}i\text{-}Pr)_4$ (**1c**)(Ph)) in a Pyrex NMR tube produces bibenzyl and toluene, in a 4:1 concentration ratio, and $W_2(\mu\text{-}C_2Et_2)_2(O\text{-}i\text{-}Pr)_4$, (**3c**). At least two other organometallic products, which have not been identified, are also formed, and **3c** represents only ca. 45% of the metal containing products. An efficient synthesis of **3c** and its spectroscopic properties are discussed in the following paper.[2] The photodecompositions of the $CH_2SiMe_3$ derivatives of **1c** were not investigated.

## Solid-State Structures, Solution Structures, Bonding Considerations, and Spectroscopic Studies

Ball-and-stick drawings of the $HW_2(\mu\text{-}CPh)(\mu\text{-}C_4Me_4)(O\text{-}i\text{-}Pr)_4$ ((**2**)H(Ph)) and $(Me_3SiCH_2)W_2(\mu\text{-}CSiMe_3)(\mu\text{-}C_4Me_4)(O\text{-}i\text{-}Pr)_4$ ((**2**)R($SiMe_3$)) molecules are shown in Figures 1 and 2, respectively. Selected bond distances and angles and fractional coordinates are listed in Tables I through IV. Summaries of the crystal data for both compounds are listed in Table V. A comparison of pertinent structural data for (**2**)H(Ph) and (**2**)R($SiMe_3$) is given in Table VI and emphasizes the structural similarities of the two compounds.

Both compounds have $C_s$ molecular symmetry in solution and virtual $C_s$ symmetry in the solid state. The M–M distances of 2.755 (2) and 2.780 (2) Å, for (**2**)H(Ph) and (**2**)R($SiMe_3$) respectively, are indicative of long W–W single bonds and the W–O distances of 1.90 Å (average) and W–O–C angles of 144° (average) are consistent with strong W–O bonds with moderate oxygen-to-metal $\pi$ bonding.

**Table III. Selected Bond Distances (Å) and Angles (deg) for $(Me_3SiCH_2)W_2(\mu\text{-}CSiMe_3)(\mu\text{-}C_4Me_4)(O\text{-}i\text{-}Pr)_4$**

| Bond Distances | | | |
|---|---|---|---|
| W(1)–W(2) | 2.780 (2) | W(2)–O(29) | 1.884 (5) |
| W(1)–O(21) | 1.934 (6) | W(2)–O(33) | 1.883 (5) |
| W(1)–O(25) | 1.916 (5) | W(2)–C(4) | 2.098 (8) |
| W(1)–C(4) | 2.439 (8) | W(2)–C(7) | 2.106 (8) |
| W(1)–C(5) | 2.489 (8) | W(2)–C(16) | 1.971 (8) |
| W(1)–C(6) | 2.510 (8) | Si(12)–C(11) | 1.891 (9) |
| W(1)–C(7) | 2.467 (8) | Si(17)–C(16) | 1.871 (8) |
| W(1)–C(11) | 2.218 (9) | C(4)–C(5) | 1.408 (10) |
| W(1)–C(16) | 1.976 (8) | C(5)–C(6) | 1.418 (11) |
| | | C(6)–C(7) | 1.410 (12) |

| Bond Angles | | | |
|---|---|---|---|
| O(21)–W(1)–O(25) | 122.09 (23) | W(2)–O(33)–C(34) | 149.6 (5) |
| O(29)–W(2)–O(33) | 97.77 (24) | W(1)–C(11)–Si(12) | 128.0 (4) |
| W(1)–O(21)–C(22) | 142.0 (5) | W(1)–C(16)–Si(17) | 147.6 (5) |
| W(1)–O(25)–C(26) | 140.7 (5) | W(2)–C(16)–Si(17) | 122.8 (4) |
| W(2)–O(29)–C(30) | 150.0 (5) | | |

**Table IV. Fractional Coordinates for $(Me_3SiCH_2)W_2(\mu\text{-}CSiMe_3)(\mu\text{-}C_4Me_4)(O\text{-}i\text{-}Pr)_4$**

| atom | $10^4x$ | $10^4y$ | $10^4z$ | $10B_{iso}$, Å$^2$ |
|---|---|---|---|---|
| W(1) | 3317.3 (3) | 2637.0 (2) | −3369.8 (3) | 11 |
| W(2) | 5615.0 (3) | 2478.4 (2) | −2278.3 (3) | 12 |
| C(3) | 4926 (7) | 4374 (6) | −1829 (9) | 19 |
| C(4) | 4632 (7) | 3445 (5) | −1591 (8) | 13 |
| C(5) | 3687 (7) | 3254 (5) | −930 (8) | 15 |
| C(6) | 3543 (7) | 2360 (5) | −764 (8) | 16 |
| C(7) | 4344 (7) | 1868 (5) | −1327 (8) | 15 |
| C(8) | 4241 (8) | 920 (6) | −1292 (9) | 20 |
| C(9) | 2934 (8) | 3899 (6) | −430 (9) | 19 |
| C(10) | 2615 (7) | 1973 (6) | −46 (9) | 19 |
| C(11) | 2521 (7) | 2539 (6) | −5628 (9) | 17 |
| Si(12) | 971 (2) | 2668 (2) | −6420 (2) | 17 |
| C(13) | 34 (8) | 2868 (7) | −5074 (11) | 30 |
| C(14) | 387 (9) | 1707 (7) | −7523 (11) | 30 |
| C(15) | 795 (8) | 3567 (6) | −7729 (10) | 26 |
| C(16) | 4702 (7) | 2417 (5) | −4191 (8) | 14 |
| Si(17) | 5334 (2) | 2178 (2) | −5810 (2) | 15 |
| C(18) | 6902 (8) | 2125 (7) | −5324 (10) | 26 |
| C(19) | 4798 (8) | 1122 (6) | −6600 (10) | 24 |
| C(20) | 5065 (8) | 3025 (6) | −7193 (10) | 23 |
| O(21) | 2328 (5) | 1659 (4) | −3201 (6) | 17 |
| C(22) | 1652 (7) | 1017 (5) | −4020 (9) | 18 |
| C(23) | 2386 (8) | 313 (6) | −4427 (10) | 24 |
| C(24) | 780 (8) | 704 (7) | −3146 (11) | 29 |
| O(25) | 2758 (5) | 3777 (3) | −3559 (6) | 16 |
| C(26) | 2394 (7) | 4393 (6) | −4613 (9) | 19 |
| C(27) | 3374 (8) | 4774 (6) | −5238 (10) | 24 |
| C(28) | 1778 (9) | 5074 (6) | −3925 (11) | 30 |
| O(29) | 6837 (5) | 3276 (3) | −2174 (6) | 16 |
| C(30) | 7637 (8) | 3849 (6) | −1369 (9) | 19 |
| C(31) | 8781 (8) | 3717 (7) | −1782 (11) | 28 |
| C(32) | 7654 (8) | 3732 (6) | 199 (10) | 24 |
| O(33) | 6481 (5) | 1488 (4) | −1915 (6) | 18 |
| C(34) | 7002 (7) | 885 (6) | −948 (9) | 20 |
| C(35) | 7133 (8) | 1220 (6) | 540 (10) | 27 |
| C(36) | 8144 (10) | 676 (8) | −1343 (12) | 40 |

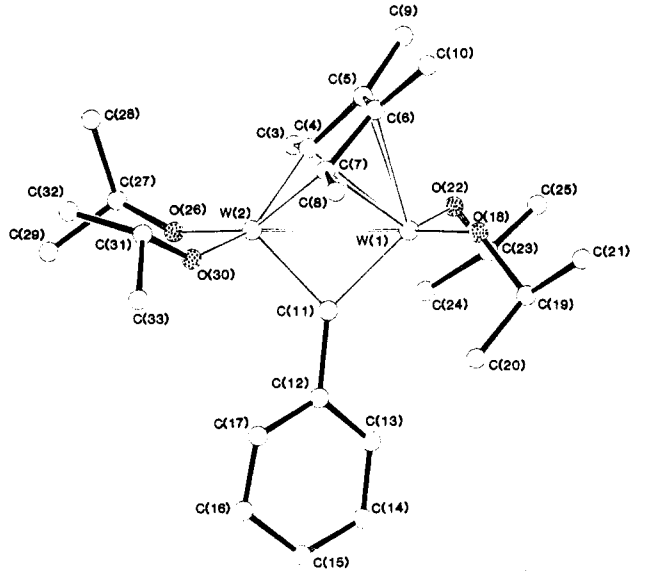


**Figure 1.** A ball-and-stick drawing of the $HW_2(\mu\text{-CPh})(\mu\text{-}C_4Me_4)(O\text{-}i\text{-Pr})_4$ molecule.

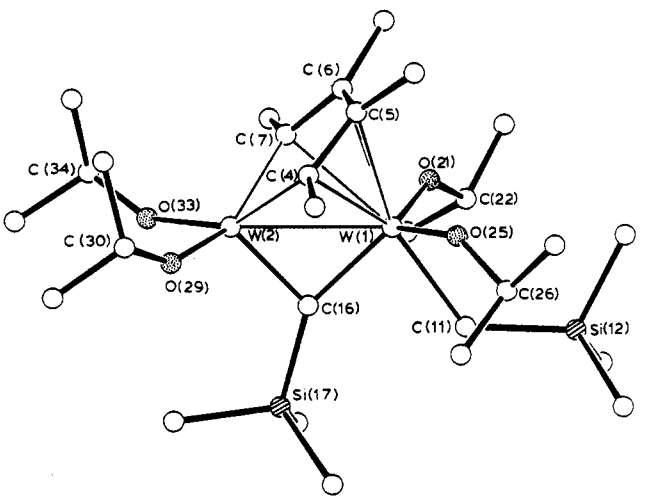


**Figure 2.** A ball-and-stick drawing of the $(Me_3SiCH_2)W_2(\mu\text{-}CSiMe_3)(\mu\text{-}C_4Me_4)(O\text{-}i\text{-Pr})_4$ molecule.

The metallacyclopentadiene rings display typical W(2)–$C_\alpha$, $\eta^4$-$C_4$-W(1), and C–C distances of 2.1 (1), 2.4 (1), and 1.4 (1) Å, respectively. The alkylidyne fragments symmetrically bridge the $W_2$ centers with W–C distances of 1.97 Å (average). The $CH_2SiMe_3$ ligand of (2)R($SiMe_3$) was located on W(1) trans to the $\eta^4$-$C_4$ ring, but the hydride ligand of (2)H(Ph) could not be detected crystallographically.

The hydride ligands of compounds (2)H are clearly terminal metal hydrides and are not attached to the bridging alkylidyne carbons (i.e. they are not alkylidenes with agostic M–H–C interactions).[6,7] This conclusion is based on the following observations. (1) The hydrogen resonances display tungsten couplings ($^1J_{^{183}W-^1H}$, 14% total satellite intensity) of 125 Hz (average). Tungsten–hydrogen couplings of this magnitude are typical of hydride ligands on tungsten alkoxide complexes.[8] (2) The C–H coupling constant between the alkylidyne carbon and the hydride is 5 Hz in (2)H($SiMe_3$) which is inconsistent with an alkylidene C–H moiety.

Spatially, the hydride ligand of (2)H(Ph) could be accommodated in the two positions shown in Figure 3. Site A would place the hydride trans to the alkylidyne carbon whereas B would leave the hydride trans to the $\eta^4$-$C_4$ ring in analogy with the $CH_2SiMe_3$ ligand of (2)R($SiMe_3$). The structural and spectroscopic similarities between (2)H(Ph) and (2)R($SiMe_3$) suggest that the hydride ligand is located

(6) Brookhart, M.; Green, M. L. H. *J. Organomet. Chem.* **1983**, *250*, 395.
(7) Bandy, J. A.; Green, M. L. H.; O'Hare, D.; Prout, K. *J. Chem. Soc., Chem. Commun.* **1984**, 1402.
(8) Chisholm, M. H.; Huffman, J. C.; Smith, C. A. *J. Am. Chem. Soc.* **1986**, *108*, 222.

**Table V. Summary of Crystallographic Data for $HW_2(\mu\text{-CPh})(\mu\text{-}C_4Me_4)(O\text{-}i\text{-Pr})_4$ and $(Me_3SiCH_2)W_2(\mu\text{-CSiMe}_3)(\mu\text{-}C_4Me_4)(O\text{-}i\text{-Pr})_4$[a]**

| | A | B |
|---|---|---|
| empirical formula | $W_2O_4C_{27}H_{46}$ | $W_2C_{28}H_{60}O_4Si_2$ |
| color of cryst | black | yellow |
| cryst dimensions (mm) | 0.08 × 0.03 × 0.05 | 0.18 × 0.18 × 0.20 |
| space group | $P2_12_12_1$ | $P\bar{1}$ |
| cell dimens | | |
| temp (°C) | −159 | −155 |
| $a$ (Å) | 9.183 (3) | 11.906 (4) |
| $b$ (Å) | 15.606 (6) | 15.633 (5) |
| $c$ (Å) | 19.977 (9) | 9.584 (3) |
| $\alpha$ (deg) | | 90.47 (2) |
| $\beta$ (deg) | | 99.49 (2) |
| $\gamma$ (deg) | | 91.27 (2) |
| $Z$ (molecules/cell) | 4 | 2 |
| $V$ (Å$^3$) | 2862.70 | 1758.93 |
| d(calcd) (gm/cm$^3$) | 1.862 | 1.738 |
| wavelength (Å) | 0.710 69 | 0.710 69 |
| mol wt | 802.36 | 920.68 |
| linear abs coeff (cm$^{-1}$) | 82.312 | 67.734 |
| detector to sample dist (cm) | 22.5 | 22.5 |
| sample to source dist (cm) | 23.5 | 23.5 |
| av $\omega$ scan width at half-height | 0.25 | 0.25 |
| scan speed (deg/min) | 4.0 | 4.0 |
| scan width (deg + dispersn) | 2.0 | 2.0 |
| individual bkgd (s) | 8 | 8 |
| aperture size (mm) | 3.0 × 4.0 | 3.0 × 4.0 |
| $2\theta$ range (deg) | 6–45 | 6–45 |
| total no. of reflctns collected | 3804 | 5173 |
| no. of unique intensities | 3710 | 4622 |
| no. of $F > 3.00\sigma(F)$ | 3204 | 4030 |
| $R(F)$ | 0.0666 | 0.0330 |
| $R_w(F)$ | 0.0617 | 0.0348 |
| goodness of fit for the last cycle | 1.335 | 0.977 |
| max $\Delta/\sigma$ for last cycle | 0.05 | 0.05 |

[a] A, $HW_2(\mu\text{-CPh})(\mu\text{-}C_4Me_4)(O\text{-}i\text{-Pr})_4$; B, $(Me_3SiCH_2)W_2(\mu\text{-CSiMe}_3)(O\text{-}i\text{-Pr})_4$.

**Table VI. Comparison of Pertinent Bond Distances (Å) and Angles (deg) for Compounds $HW_2(\mu\text{-CPh})(\mu\text{-}C_4Me_4)(O\text{-}i\text{-Pr})_4$ and $(Me_3SiCH_2)W_2(\mu\text{-CSiMe}_3)(\mu\text{-}C_4Me_4)(O\text{-}i\text{-Pr})$**

| | A[a] | B[a] |
|---|---|---|
| | Bond Distances[b] | |
| W–W | 2.755 (2) | 2.780 (2) |
| W–O | 1.90 (4) | 1.88 (1)/1.92 (2) |
| W(1)–C(ring) | 2.44 (6) | 2.48 (5) |
| W(2)–$C_\alpha$(ring) | 2.09 (3) | 2.10 (1) |
| W–C(alkylidyne) | 1.96 (4) | 1.97 (1) |
| | Bond Angles[b] | |
| W–O–C | 141 (14) | 146 (7) |
| O–W(1)–O | 115 (1) | 122 (1) |
| O–W(2)–O | 98 (1) | 98 (1) |
| W(1)–C–X(alkylidyne) | 140 (2) | 128 (1) |
| W(2)–C–X(alkylidyne) | 131 (2) | 123 (1) |

[a] A, $HW_2(\mu\text{-CPh})(\mu\text{-}C_4Me_4)(O\text{-}i\text{-Pr})_4$; B, $(Me_3SiCH_2)W_2(\mu\text{-CSiMe}_3)(\mu\text{-}C_4Me_4)(O\text{-}i\text{-Pr})_4$. [b] Averaged where appropriate.

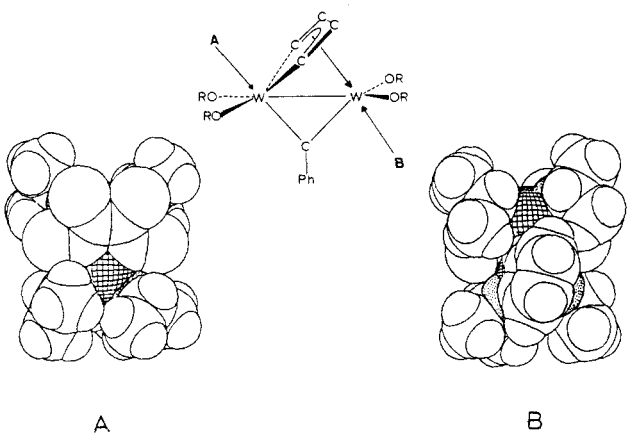


**Figure 3.** Space-filling diagrams of the $HW_2(\mu\text{-CPh})(\mu\text{-}C_4Me_4)(O\text{-}i\text{-Pr})_4$ molecule showing the two potential sites for the hydride ligand. The hatched areas represent exposed tungsten, and the speckled areas represent oxygen.

**Table VII. Percent Signal Enhancements for NOE Difference Experiments[a] on $HW_2(\mu\text{-CPh})(\mu\text{-}C_4Me_4)(O\text{-}i\text{-Pr})_4$**

| presaturated nucleus[b] | obsd enhancements (%)[b] | | |
|---|---|---|---|
| | $H_A$ | $H_B$ | $H_C$ |
| $H_A$ | | 16 | 10 |
| $H_B$ | 22 | | |
| $H_C$ | 9 | | |

[a] See Experimental Section for procedural details. [b] $H_A$, hydride; $H_B$, O-*i*-Pr methine hydrogen on W(1); $H_C$, ortho C*Ph* hydrogens.

**Table VIII. $T_1$ Relaxation Times[a] for Pertinent Hydrogen Atoms in $HW_2(\mu\text{-CPh})(\mu\text{-}C_4Me_4)(O\text{-}i\text{-Pr})_4$**

| hydrogen nucleus | $T_1$ (s) | hydrogen nucleus | $T_1$ (s) |
|---|---|---|---|
| hydride | 0.50 | OC*H*Me$_2$ [on W(1)] | 1.1 |
| ortho ($\mu$-C*Ph*) | 1.6 | OC*H*Me$_2$ [on W(2)] | 1.6 |
| meta ($\mu$-C*Ph*) | 2.5 | OCH*Me*$_2$ [on W(1)] | 0.6 |
| | | OCH*Me*$_2$ [on W(2)] | 0.9 |

[a] $T_1$ values were estimated from $\tau_{null}$ data by using the relationship $T_1 = \tau_{null}/\ln 2$. Experimental details are listed in the Experimental Section.

at site B. This assignment was confirmed by NOE difference NMR studies.[9] A schematic drawing of (2)H(Ph) emphasizing the optimum orientation of the pertinent hydrogen atoms is shown by IV. The hydride ligand ($H_A$),

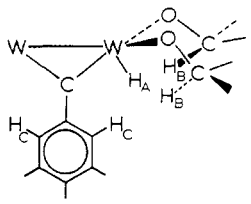


IV

the methine O-*i*-Pr hydrogens of W(1) ($H_B$), and the ortho hydrogens of the benzylidyne fragment ($H_C$) are all relatively close in certain rotameric conformations. Significant enhancements of the O-*i*-Pr methine ($H_B$) and ortho benzylidyne ($H_C$) $^1H$ NMR resonances are observed when the hydride signal is presaturated. Similarly, the hydride resonance is enhanced when either $H_B$ or $H_C$ are presaturated. Moreover, the resonances of the meta and para benzylidyne hydrogens and the O-*i*-Pr methine hydrogens of W(2) are not detectably enhanced upon hydride presaturation. The relative enhancements and pertinent $T_1$ relaxation times for (2)H(Ph) are listed in Tables VII and VIII, respectively. These data reliably establish that the hydride ligand resides at site B trans to the $\eta^4$-$C_4$ ring.

(9) Crabtree, R. H.; Segmuller, B. E.; Uriarte, R. J. *Inorg. Chem.* **1985**, *24*, 1949.

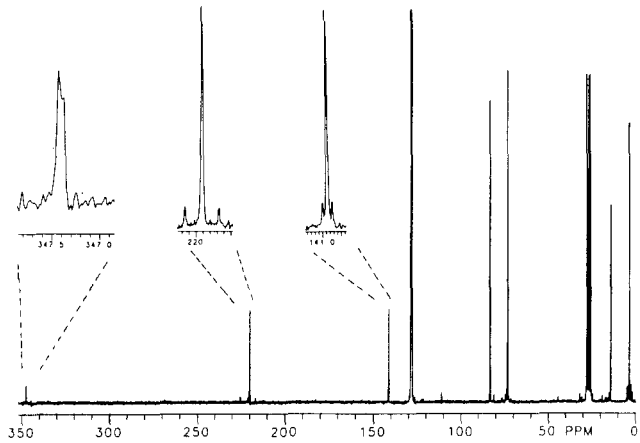


**Figure 4.** $^{13}C\{^1H\}$ NMR spectrum of $HW_2(\mu\text{-CSiMe}_3)(\mu\text{-}C_4Me_4)(O\text{-}i\text{-Pr})_4$ recorded in benzene-$d_6$ at 22 °C and 75 MHz. Only the proton resonances between 0 and 10 ppm were decoupled with the hydride ($\delta$ +20.7) carbon coupling being unaffected.

The local geometry about W(2) in both compounds is distorted square-pyramidal with the alkylidyne ligand occupying the apical position. The geometry about W(1) is trigonal-bipyramidal if the $\eta^4$-$C_4$ ring is assumed to occupy a single coordination site. The $W_2^{10+}$ core can be viewed as a $d^1$–$d^1$ or $d^0$–$d^2$ dinuclear unit depending upon formal charge assignment in the $W_2(\mu\text{-CR})$ fragment. Two valence-bond descriptions are depicted by V and VI. The similarities in W(1)–C(alkylidyne) and W(2)–C(alkylidyne) bond distances are indicative of equal contributions from both resonance structures.

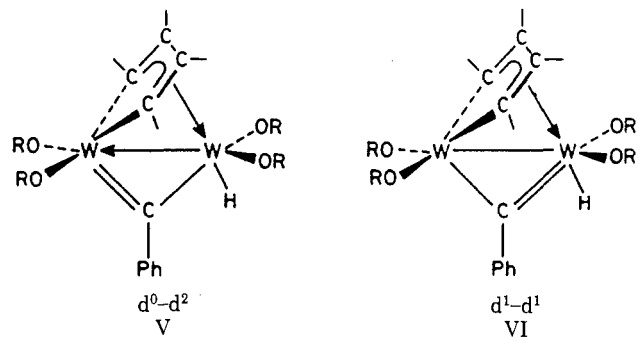


The $^1H$ and $^{13}C\{^1H\}$ NMR data for compounds **2** are listed in Table IX, and the IR data are given in the Experimental Section. The limiting $^1H$ and $^{13}C\{^1H\}$ NMR spectra for **2** are consistent with the solid-state structures just described. The $^{13}C\{^1H\}$ NMR spectrum of (2)H($SiMe_3$) is shown in Figure 4 as a representative of compounds **2**. The NMR spectra of **2** reveal two types of O-*i*-Pr ligands each having diastereotopic methyl groups. The O-*i*-Pr methine hydrogens of (2)H(Ph) have moderately long $T_1$ relaxation times of 1.4 s (average) requiring long interacquisition delays (ca. 6s) for accurate FT $^1H$ NMR integrations. The $MC_4$ metallacyclopentadiene rings are static on the NMR time scale from −80 to +80 °C in toluene-$d_8$. Sharp singlets are observed for the $\alpha$- and $\beta$-methyl groups of the $C_4$ ring in both the $^1H$ and $^{13}C\{^1H\}$ NMR spectra. The $\alpha$ ring carbons appear at 220 ppm (average) and typically display tungsten–carbon couplings ($^1J_{^{183}W-^{13}C}$, 14% total satellite intensity) of 74 Hz (average). The alkylidyne carbons have $^{13}C$ NMR chemical shifts of 340 ppm (average), but no W–C couplings have been observed to date

**Table IX. NMR Data[a] for $HW_2(\mu\text{-}CR)(\mu\text{-}C_4Me_4)(O\text{-}i\text{-}Pr)_4$ and $(Me_3SiCH_2)W_2(\mu\text{-}CSiMe_3)(\mu\text{-}C_4Me_4)(O\text{-}i\text{-}Pr)_4$**

| compound | $^1H$ NMR[b,c] | $^{13}C\{^1H\}$ NMR[d] |
|---|---|---|
| $(Me_3SiCH_2)W_2(\mu\text{-}CSiMe_3)(\mu\text{-}C_6Me_4)(O\text{-}i\text{-}Pr)_4$ (benzene-$d_6$, 22 °C) | OC*H*Me$_2$ (5.11, sept, 2 H, 6.1), (4.52, sept, 2 H, 6.1); C$_4$*Me*$_4$ (2.10, s, 6 H), (1.76, s, 6 H); OCH*Me*$_2$ (1.47, d, 6 H, 6.1), (1.28, d br, 6 H, 6.1), (1.23, d, 6 H, 6.1), (0.84, d br, 6 H, 6.1); $CH_2SiMe_3$ and $\mu$-CSi*Me*$_3$, (0.74, s, 9 H, $^2J_{^{29}Si\text{-}^1H}$ = 6.8), (0.48 s, 9 H, $^2J_{^{29}Si\text{-}^1H}$ = 6.1) | $\mu$-*C*SiMe$_3$ (347.7); $\mu$-*C*$_4$Me$_4$, $\alpha$ (212.7); $\mu$-*C*$_4$Me$_4$, $\beta$ (141.3); OCHMe$_2$ (73.4, $^2J_{^{183}W\text{-}^{13}C}$ = 10), (73.0); *C*H$_2$SiMe$_3$ (44.3); OCH*Me*$_2$ and $\mu$-C$_4$*Me*$_4$ (27.9), (27.6), (27.4), (25.7), (25.2), (15.0); CH$_2$Si*Me*$_3$ and $\mu$-CSi*Me*$_3$ (5.1), (4.4) |
| $HW_2(\mu\text{-}CSiMe_3)(\mu\text{-}C_4Me_4)(O\text{-}i\text{-}Pr)_4$ (benzene-$d_6$, 22 °C) | W–*H* (20.67, s, 1 H, $^1J_{^{183}W\text{-}^1H}$ = 127.6); OC*H*Me$_2$ (5.28, sept, 2 H, 6.1), (4.52, sept, 2 H, 6.1); C$_4$*Me*$_4$ (2.15, s, 6 H), (1.55, s, 6 H); OCH*Me*$_2$ (1.40, d, 6 H, 6.1), (1.34, d, 6 H, 6.1), (1.24, d, 6 H, 6.1), (0.90, d, 6 H, 6.1); CSi*Me*$_3$ (0.74, s, 9 H) | $\mu$-CSiMe$_3$ (347.4); $\mu$-C$_4$Me$_4$, $\alpha$ (219.8, $^1J_{^{183}W\text{-}^{13}C}$ = 19); OCHMe$_2$ (83.1, $^2J_{^{183}W\text{-}^{13}C}$ = 11), (73.0, $^2J_{^{183}W\text{-}^{13}C}$ = 9), OCH*Me*$_2$ and $\mu$-C$_4$*Me*$_4$ (27.6), (26.9), (26.2), (26.1), (25.4), (14.0); $\mu$-CSi*Me*$_3$ (3.2) |
| $HW_2(\mu\text{-}C\text{-}t\text{-}Bu)(\mu\text{-}C_4Me_4)(O\text{-}i\text{-}Pr)_4$ (benzene-$d_6$, 22 °C) | W–*H* (19.77, s, 1 H, $^1J_{^{183}W\text{-}^1H}$ = 125.0); OC*H*Me$_2$ (5.29, sept, 2 H, 6.1), (4.51, sept, 2 H, 6.1); C$_4$*Me*$_4$ (2.15, s, 6 H); CC*Me*$_3$ (1.96, s, 9 H); C$_4$*Me*$_4$ (1.55, s, 6 H); OCH*Me*$_2$ (1.38, dd, 12 H, 6.1), (1.23, d, 6 H, 6.1), (0.90, d, 6 H, 6.1) | $\mu$-*C*CMe$_3$ (364.0); *C*$_4$Me$_4$, $\alpha$ (220.2); *C*$_4$Me$_4$, $\beta$ (140.6, $^2J_{^{183}W\text{-}^{13}C}$ = 19); OCHMe$_2$ (83.1), (72.9); $\mu$-*C*CMe$_3$ (53.0); $\mu$-CC*Me*$_3$ (36.3); OCH*Me*$_2$ (27.5), (26.9), (26.2), (25.4); C$_4$*Me*$_4$ (26.1), (14.0) |
| $HW_2(\mu\text{-}CPh)(\mu\text{-}C_4Me_4)(O\text{-}i\text{-}Pr)_4$; $^1H$ NMR (toluene-$d_8$, −40 °C), $^{13}C\{^1H\}$ NMR (toluene-$d_8$, 22 °C) | W–*H* (20.35, s, 1 H, $J^{183}_{W\text{-}^1H}$ = 124.4); CH$_2$*Ph*, ortho (8.56, d, 2 H, 7.2); CH$_2$*Ph*, meta (7.55, dd, 2 H, 7.2); CH$_2$*Ph*, para (~7.0, t, 1 H); OC*H*Me$_2$ (5.39, sept, 2 H, 6.1), (4.48, sept, 2 H, 6.1); C$_4$*Me*$_4$ (2.19, s, 6 H), (168, s, 6 H; OCH*Me*$_2$ (1.40, d, 6 H, 6.1), (1.29, d, 6 H, 6.1), (120, d, 6 H, 6.1), (0.86, d, 6 H, 6.1) | $\mu$-*C*Ph (341.4); *C*$_4$Me$_4$, $\alpha$ (221.0, $J^{183}_{W\text{-}^{13}C}$ = 72); C*Ph*, ipso (154.7); C$_4$Me$_4$, $\beta$ (141.2); OCHMe$_2$ (82.5), (73.3); OCH*Me*$_2$ (27.5), (26.9), (26.4), (25.6); C$_4$*Me*$_4$ (~21), (14.0) |

[a] $^1H$ NMR data are reported as follows: assignment (chemical shift in ppm, multiplicity, relative intensity, H–H coupling constant in Hz, heteronuclear coupling constants in Hz). $^{13}C\{^1H\}$ NMR data are reported as follows: assignment (chemical shift in ppm, heteronuclear coupling constants in Hz). [b] Abbreviations: s, singlet; d, doublet; t, triplet; sept, septet; br, broad. [c] Assignments were based on selective decoupling experiments in conjunction with NOE difference studies. [d] Assignments were based on proton-coupled $^{13}C$ NMR experiments when ambiguities existed.

due to the low relative signal intensity of the alkylidyne resonances. For (2)H(SiMe$_3$), the two-bond, hydride alkylidyne-carbon coupling constant ($^2J_{^{13}C\text{-}^1H}$) is 5 Hz (see Figure 4). Rotation about the alkylidyne C–Ph bond in (2)H(Ph) is rapid on the NMR time scale even at −80 °C.

The hydride ligands of compounds (2)H display $^1H$ NMR resonances at ca. 20 ppm *downfield* of SiMe$_4$ with tungsten–hydrogen couplings ($^1J_{^{183}W\text{-}^1H}$, 14% total satellite intensity) of 125 Hz (average). The factors influencing the hydride chemical shifts are not entirely clear but anisotropies associated with the O-*i*-Pr W←O multiple bonds could contribute to the anomalous deshielding. The hydride ligand of (2)H(Ph) has a $T_1$ relaxation time of 500 ms, and no $T_1$ differences between the $^{183}W$–*H* and $^xW$–*H* isotopimers were detected (i.e. the tungsten satellites have a $T_1$ equal to that of the central resonance).[9] The $\alpha$-carbon of the CH$_2$SiMe$_3$ ligand in (2)R(SiMe$_3$), however, is not unusually deshielded as might have been anticipated. The CH$_2$SiMe$_3$ $\alpha$-hydrogens were not observed in the $^1H$ NMR spectrum, but the proton-coupled $^{13}C$ NMR spectrum revealed a triplet ($^1J_{^{13}C\text{-}^1H}$ = 114 Hz) for the CH$_2$SiMe$_3$ $\alpha$-carbon, thus verifying their existence.

Compounds **2** are dynamic in solution and a fluxional process involving the O-*i*-Pr ligands on W(2) is observed by $^1H$ NMR at room temperature for (2)H(Ph) and (2)R(SiMe$_3$). The two doublets for the diastereotopic O-*i*-Pr methyl groups of (2)H(Ph) broaden at room temperature, coalesce into the base line at ca. +60 °C, and do not reemerge even at +90 °C. The resonances for the remaining groups, including the O-*i*-Pr ligands on W(1), are essentially unaffected by temperature. This dynamic behavior *cannot* be attributed to a simple turnstile pseudorotation as outlined in Scheme III. A pseudorotation of this type would not exchange the diastereotopic O-*i*-Pr methyl groups and would, in fact, be invisible by $^1H$ NMR spectroscopy. Inversion of configuration at W(2) must be invoked to exchange the diastereotopic O-*i*-Pr methyl groups. One possible process is outlined in Scheme IV.

**Scheme III**

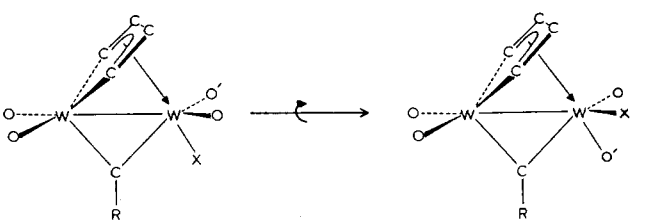


The IR spectra of compounds (2)H show broad, medium-intensity bands at ca. 1875 cm$^{-1}$ assignable to terminal W–H stretching modes.

## Mechanistic Considerations

The thermal reactions of bis(alkyne) compounds **1a**, outlined in Scheme I, and $W_2(CH_2R)_2(EtCCEt)_2(O\text{-}i\text{-}Pr)_4$ (**1c**) were investigated as a function of the alkyl (R) and alkyne (R′, R″) substituents. The study was designed to probe the nature of $\alpha$-hydrogen activation, alkyne coupling,

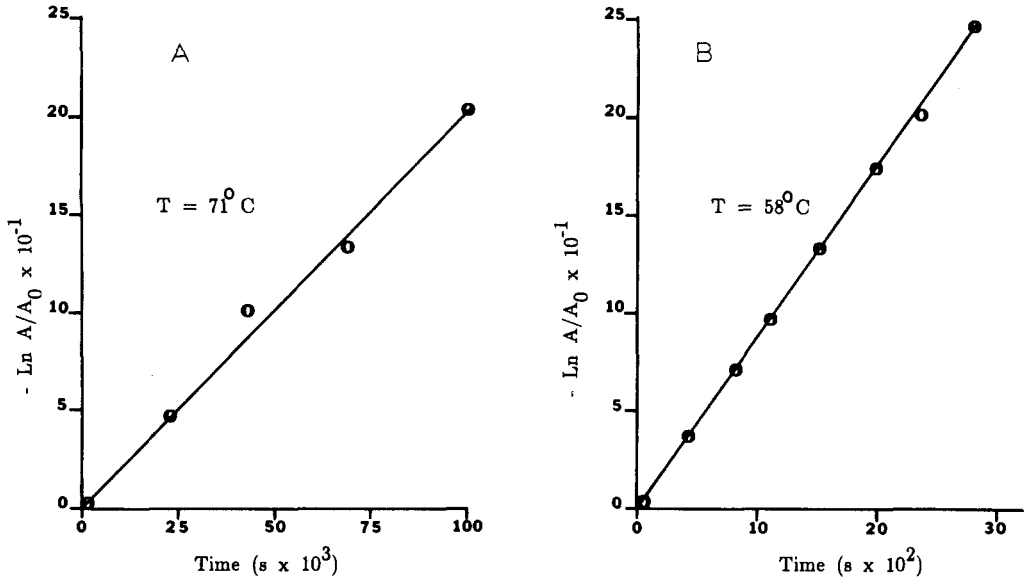


**Figure 5.** Plots of ln $(A/A_0)$ versus time (s) for the thermolyses of compounds $W_2(EtCCEt)_2(CH_2SiMe_3)_2(O\text{-}i\text{-}Pr)_4$ (A) and $W_2(MeCCMe)_2(CH_2SiMe_3)_2(O\text{-}i\text{-}Pr)_4$ (B) at 71 and 58 °C, respectively.

Scheme IV

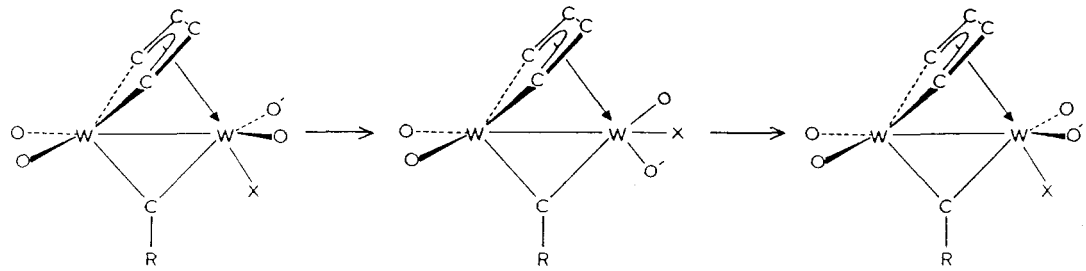

O = O-*i*-Pr

and the order of events in the reaction sequences. In related systems involving phosphine-promoted α-hydrogen activation in $W_2(CH_2R)_2(O\text{-}i\text{-}Pr)_4(PMe_3)_2(W{\equiv}W)$ complexes, phosphine dissociation precedes the C–H abstraction process which may involve metal-to-metal alkyl migration.[10] The present study indicates that alkyne dissociation and metal-to-metal alkyl migration are not involved in the reactions outlined in Scheme I. The data are most consistent with an intramolecular α-hydrogen abstraction in which preceding steps involving alkyne coupling are rate-determining.

Thermolysis studies in $C_6D_6$ solvents show that the decompositions of the bis(alkyne) compounds are first-order in **1a** or **1c** over several half-lives. Representative first-order rate plots for (**1a**)($SiMe_3$) and (**1c**)($SiMe_3$) are shown in Figure 5. A list of pertinent rate constants is given in Table X.

The rate of decomposition of $W_2(CH_2SiMe_3)_2(MeCCMe)_2(O\text{-}i\text{-}Pr)_4$ ((**1a**)($SiMe_3$)) is unaffected by a 6-fold excess of MeC≡CMe (see runs 9 and 11, Table X). Crossover experiments, outlined in eq 2 and 3, show that

$$W_2(CH_2R)_2(MeCCMe)_2(O\text{-}i\text{-}Pr)_4 + \text{excess } EtC{\equiv}CEt \xrightarrow[\Delta]{} \text{no crossover} \quad (2)$$

$$W_2(CH_2R)_2(EtCCEt)_2(O\text{-}i\text{-}Pr)_4 + \text{excess } MeCCMe \xrightarrow[\Delta]{} \text{no crossover} \quad (3)$$

thermolysis of compounds **1a** or **1c** in the presence of excess "crossover acetylene" does not result in incorporation of the external alkyne into the starting materials **1** or the final products **2**. Thus, the alkyne ligands of compounds **1a** and **1c** do not dissociate during thermolysis either in a rapid preequilibrium step or in a process occurring in or after the rate-determining step. This behavior contrasts the inverse phosphine dependence in the related α-hydrogen abstraction process involving $W_2(CH_2Ph)_2(O\text{-}i\text{-}Pr)_4(PMe_3)_2$.[10]

Thermolysis of $W_2(CD_2C_6D_5)_2(MeCCMe)_2(O\text{-}i\text{-}Pr)_4$ ((**1a**)(Ph-$d_7$)) generates $DW(\mu\text{-}CC_6D_5)(\mu\text{-}C_4Me_4)(O\text{-}i\text{-}Pr)_4$ and toluene-$d_8$. No W–*H* species or toluene-$d_7$ were detected.[11] When a 1:1 (mol %) mixture of (**1a**)(Ph) and

**Table X. First-Order Rate Constants[a] for the Thermolysis of Compounds $W_2R_2(R'CCR')_2(O\text{-}i\text{-}Pr)_4$**

| run | R | R′ | temp (°C) | $k$ ($s^{-1}$) |
|---|---|---|---|---|
| 1 | Ph | Me | 61 | 2.1 (2) × $10^{-5}$ |
| 2 | | | 74 | 9.0 (2) × $10^{-5}$ |
| 3 | | | 85 | 2.5 (3) × $10^{-4}$ |
| 4 | Ph-$d_7$ | Me | 61 | 1.5 (1) × $10^{-5}$ |
| 5 | Ph | Et | 71 | 1.1 (3) × $10^{-5}$ |
| 6 | Ph-$d_7$ | Et | 71 | 3.5 (4) × $10^{-6}$ |
| 7 | $SiMe_3$ | Me | 38 | 1.1 (2) × $10^{-4}$ |
| 8 | | | 48 | 3.2 (1) × $10^{-4}$ |
| 9 | | | 57 | 9.5 (5) × $10^{-4}$ |
| 10 | | | 67 | 2.1 (3) × $10^{-3}$ |
| 11 | $SiMe_3$ | Me[b] | 57 | 9.8 (3) × $10^{-4}$ |
| 12 | $SiMe_3$ | Et | 71 | 2.4 (4) × $10^{-5}$ |

[a] Rate constants were measured in $C_6D_6$ solutions using $^1H$ NMR spectroscopy. See Experimental Section for procedural details. [b] In the presence of a 6-fold excess of MeC≡CMe.

(10) Blau, R. J.; Chisholm, M. H.; Eichhorn, B. W.; Folting, K.; Huffman, J. C., manuscript in preparation.

Scheme V

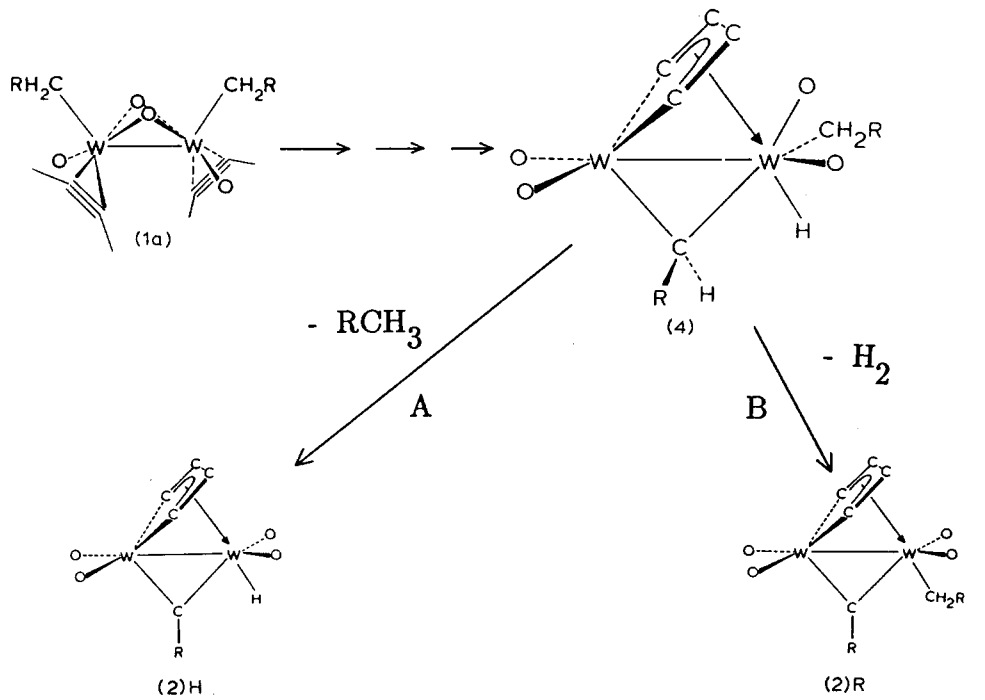


(**1a**)(Ph-$d_7$) are thermolyzed in $C_6D_6$, toluene and toluene-$d_8$ are produced without the formation of significant quantities of toluene-$d_1$ or toluene-$d_7$.[11] Thermolysis of (**1a**)(Ph) also does not generate bibenzyl as an organic byproduct in contrast to the low-temperature photochemical reactions described earlier. These data indicate that the hydrogen-atom transfers occur intramolecularly and free benzyl radicals are not involved.

A comparison of thermolysis rate constants for (**1a**)(Ph-$d_7$) and (1)(Ph) shows a small kinetic isotope effect, $k_H/k_D = 1.4 \pm 0.2$, at 61 °C in $C_6D_6$. Compound (**1c**)(Ph-$d_7$) displays a much larger kinetic isotope effect, $k_H/k_D = 3.1 \pm 0.5$, at 71 °C consistent with two different modes of decomposition for compounds **1a** and **1c**. Whereas C–H activation seems to be rate determining for (**1c**)(Ph), it apparently contributes less to the overall rate expression for (**1a**)(Ph).

The rates of thermolysis of 1 *decrease* with the decreasing steric demands of the alkyl groups R such that $k_{t\text{-Bu}} > k_{SiMe_3} > k_{Ph}$ (Table X, runs 1 and 9). For example, (**1a**)(*t*-Bu) cannot be detected by $^1H$ NMR at −80 °C, but (**1a**)(Ph) has a half-life of ca. 8 h at +60 °C. Electronically, $CH_2SiMe_3$ is the most electron-releasing[13] alkyl ligand in the series of three yet the rate of decomposition of $W_2(CH_2SiMe_3)_2(MeCCMe)_2(O\text{-}i\text{-}Pr)_4$ ((**1a**)($SiMe_3$)) is intermediate between that of (**1a**)(Ph) and (**1a**)(*t*-Bu). The steric bulk of the alkyl ligands follows the series $CH_2$-*t*-Bu > $CH_2SiMe_3$ > $CH_2Ph$ and parallels the observed rates of reaction.[12] Thus the differences in rates resulting from variations of the alkyl group R appear to be steric and not electronic[13] in origin. The corresponding EtCCEt analogues (**1c**)(R = Ph or $SiMe_3$) decompose up to $10^2$ times *slower* than their MeCCMe counterparts (**1a**)(R = Ph or $SiMe_3$). Thus the rates of thermolysis of **1a** and **1c** *increase* with decreasing steric demands of the alkyne substituents R′ and R″. This observation contrasts the commonly observed steric acceleration in other α-C–H activation processes caused by increasing the steric demands at the metal center.[14]

Activation parameters for the thermolyses of (**1a**)($SiMe_3$) and (**1a**)(Ph) (Figure 6) reveal a similar degree of transition-state ordering ($\Delta S^\ddagger = -9 \pm 2$ eu) for both compounds and suggest that the differences in rate are enthalpic in origin ($\Delta\Delta H^\ddagger = 2$ kcal mol$^{-1}$). Furthermore, the small negative $\Delta S^\ddagger$ values are consistent with alkane or $H_2$ elimination after the rate-determining step.

Together these results lead us to suggest that compounds **1a** decompose by rate-determining alkyne coupling that is followed by α-C–H abstraction. Increasing the steric demands of the alkyne ligands makes head-to-head alkyne coupling more difficult. For the EtCCEt analogues, **1c**, the barrier to alkyne coupling ($\Delta G^\ddagger$) is large enough to force alternate modes of decomposition other than those outlined in Scheme I. These alternate reaction pathways manifest themselves in the absence of ($\mu$-$C_4Et_4$) analogues of **2** and rate-determing C–H activations ($k_H/k_D = 3.1$ vs $k_H/k_D = 1.4$ for **1a**). Compounds **1** show a steric acceleration of alkyne coupling as a result of increasing the size of the alkyl substituents R. This acceleration apparently results from a ground-state destabilization that is responsible for the 2 kcal mol$^{-1}$ difference in activation enthalpy ($\Delta H^\ddagger$) between (**1a**)(Ph) and (**1a**)($SiMe_3$). Finally, compounds (**2**)R and (**2**)H are most likely derived from a common intermediate that possesses both an alkyl and a hydride ligand. A reaction scheme consistent with the data just discussed is presented in Scheme V. Formation of the *alkylidene* intermediate 4 is accomplished by rate-determining coupling of alkyne ligands followed by an oxidative addition of a single α-C–H. Clearly, several

(11) Trace amounts of $C_6D_5CD_2H$ were observed in certain cases. The $CD_2C_6D_5$ ligands were prepared from toluene-$d_8$ (99.5% D). Residual protio impurities in the parent toluene-$d_8$ could account for the trace amounts of $C_6D_5CD_2H$ observed in these reactions. Furthermore, any kinetic isotope effect in the α-hydrogen abstraction step would enhance the relative amount of $C_6D_5CD_2H$ with respect to the original toluene-$d_8$.

(12) (a) Rupprecht, G. A.; Messerle, L. W.; Fellmann, J. D.; Schrock, R. R. *J. Am. Chem. Soc.* **1980**, *102*, 6236. (b) Schrock, R. R.; Edwards, D. S. *J. Am. Chem. Soc.* **1982**, *104*, 6806.

(13) Wiberg, K. B. *Physical Organic Chemistry*; Wiley: New York, 1964, pp 414–415.

(14) Schrock, R. R. *Acc. Chem. Res.* **1979**, *12*, 98.

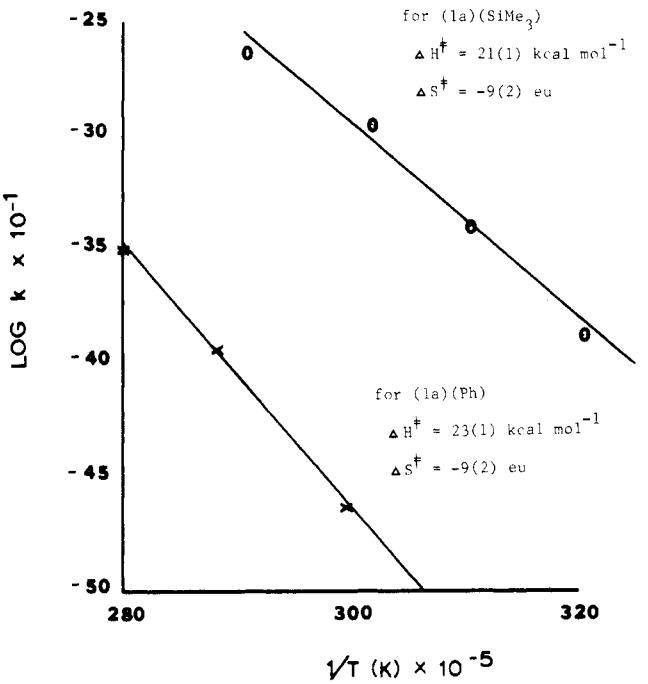


**Figure 6.** Arrhenius plots for compounds $W_2(CH_2SiMe_3)_2(MeCCMe)_2(O\text{-}i\text{-}Pr)_4$ and $W_2(CH_2Ph)_2(MeCCMe)_2(O\text{-}i\text{-}Pr)_4$ denoted by O's and X's, respectively.

elementary steps are involved in this reaction sequence, and we can only determine which process is occurring first. Intermediate **4** can eliminate $H_2$ via a four-center mechanism, involving the alkylidene $\alpha$-H and the hydride ligand, to generate the alkyl alkylidyne compound (**2**)R. Alternatively, **4** can liberate alkane ($RCH_3$) to generate (**2**)H by a similar four-center process or by reductive elimination of the alkyl and hydride functions and a subsequent oxidative addition of the alkylidene $\alpha$-H. Scheme V represents the least motion process for converting **1a** into (**2**)R and (**2**)H. Attempts to isolate an example of **4** employing analogues of **1a** that contain alkyl ligands with one $\alpha$- and no $\beta$-hydrogens have been unsuccessful thus far.[15]

## Comparison with Related CH Activations

It is interesting to compare these results with the elegant work recently reported by Bercaw and co-workers[16] concerning intramolecular C–H activation in $Cp^*_2Hf(CH_2Ph)_2$ (**5**). The authors have shown, through a series of labeling studies, that at least three separate C–H activation steps are involved in the thermal conversion of **5** to the final product $Cp^*_2\overline{HfCH_2\text{-}o\text{-}C_6H_4}$ (**6**) (eq 4). The first and

$$\underset{\mathbf{5}}{Cp^*_2Hf(CH_2Ph)_2} \rightarrow \underset{\mathbf{6}}{Cp^*_2\overline{HfCH_2\text{-}o\text{-}C_6H_4}} + \text{toluene} \quad (4)$$

rate-determining step (RDS) of the reaction apparently involves an abstraction of a $CH_2Ph$ $\alpha$-hydrogen as evidenced by the kinetic isotope effect ($k_H/k_D$) of 3.1 (2) at 140 °C observed when $\alpha$-deuteriated benzyl ligands ($CD_2C_6H_5$) were employed. Orthometalation of the benzyl ligand occurs after the RDS; thus deuteriation of benzyl ortho hydrogens ($CH_2C_6D_5$) had no effect on the rate of reaction 4 ($k_H/k_D$ = 1.1 (1)). The implicated intermediate $Cp^*(\eta^5,\eta^1\text{-}C_5Me_4CH_2)Hf(CH_2Ph)$ (**7**) was prepared independently[16] to probe the nature of the reaction steps occurring subsequent to the rate-limiting $\alpha$-H abstraction. In contrast to reaction 4, the thermal conversion of **7** to **6**, shown in eq 5, displayed a large kinetic isotope effect

$$\underset{\mathbf{7}}{Cp^*(\eta^5,\eta^1\text{-}C_5Me_4CH_2)Hf(CH_2Ph)} \rightarrow \underset{\mathbf{6}}{Cp^*_2\overline{HfCH_2\text{-}o\text{-}C_6H_4}} \quad (5)$$

when the ortho-deuteriated benzyl ligand ($CH_2C_6D_5$) was employed ($k_H/k_D$ = 9.6 at 59 °C). Thus the rate dependence on isotopic substitution in eq 5 is completely masked in eq 4 by the preceding $\alpha$-H abstraction step which is rate-limiting. Presumably, the formation of (**2**)H(Ph) could also show a significant kinetic isotope effect (i.e. $k_H/k_D \geq 4$) if the rate-determining alkyne-coupling step could be bypassed. The observed kinetic isotope effect in the thermolysis of (**1c**)(Ph-$d_7$) supports this postulate ($k_H/k_D$ = 3.1 (5) at 71 °C).

In a closely related system involving quinuclidene-promoted $\alpha$-hydrogen abstractions in $W_2(CH_2Ph)_2(O\text{-}i\text{-}Pr)_4$-(W≡W), outlined in eq 6, a kinetic isotope effect ($k_H/k_D$)

$$W_2(CH_2Ph)_2(O\text{-}i\text{-}Pr)_4 + 2Quin \rightarrow W_2(\mu\text{-}H)(\mu\text{-}CPh)(O\text{-}i\text{-}Pr)_4(Quin)_2 + \text{toluene} \quad (6)$$

of 5.0 was observed at 25 °C indicative of rate-limiting C–H activation.[10] Furthermore, significant selectivity between H and D isotopes was observed in M–H–C interactions occurring across the Os–Os bond in $HOs_3(CH_3)(CO)_{10}$.[17]

Finally, it is worth noting that the formation of compounds (**2**)H in Scheme I closely resembles the reaction outlined in eq 7 reported by Rothwell and Coffindaffer[18]

$$1,2\text{-}Mo_2(OC_6H_3Me_2)_2(CH_2SiMe_3)_4 + 2py \rightarrow SiMe_4 + Mo_2(\mu\text{-}H)(\mu\text{-}CSiMe_3)(OC_6H_3Me_2)_2(CH_2SiMe_3)_2(py)_2 \quad (7)$$

involving the thermal conversion of $1,2\text{-}Mo_2(OC_6H_3Me_2)_2(CH_2SiMe_3)_4$ to $Mo_2(\mu\text{-}CSiMe_3)(\mu\text{-}H)(CH_2SiMe_3)_2(OC_6H_3Me_2)_2(py)_2$. Reaction 7 also represents a double $\alpha$-H abstraction of one alkyl ligand in which a $\mu$-alkylidene intermediate was proposed.

## Conclusions

Bis(alkyne) complexes of formula $W_2(CH_2R)_2(MeCCMe)_2(O\text{-}i\text{-}Pr)_4$ (**1a**) react thermally in hydrocarbon solutions to form alkylidyne-bridged compounds of formula $XW_2(\mu\text{-}CR)(\mu\text{-}C_4Me_4)(O\text{-}i\text{-}Pr)_4$ (**2**) where X = $CH_2R$ or H. The products are formed from competitive double $\alpha$-hydrogen activation reactions that liberate molecular $H_2$ and $RCH_3$, respectively. Mechanistic studies indicate that the coupling of terminal alkyne ligands of **1a** are rate-determining in the conversions to compounds **2**. These competitive reactions are operative for (**1a**)($SiMe_3$) in the solid state producing 2:1 mixtures of (**2**)H($SiMe_3$) to (**2**)R($SiMe_3$) with $t_{1/2} \approx 100$ days at room temperature. Related bis(alkyne) complexes **1b** and **1c** with MeCCEt and EtCCEt alkyne ligands, respectively, are much more thermally robust in hydrocarbon solutions than compounds **1a**. Different modes of thermal activations are operative in these systems, and no analogs of **2** with $MC_4$ metallacycles bearing Et substituents have been unequivocally identified. The benzyl derivatives of **1a** and **1c** are photochemically reactive toward benzyl radical elimination producing bridging alkyne complexes of formula $W_2(\mu\text{-}C_2R'_2)_2(O\text{-}i\text{-}$

(15) Chisholm, M. H.; Eichhorn, B. W.; Folting, K.; Huffman, J. C. *Inorg. Chim. Acta* **1988**, *144*, 193.
(16) Bulls, R. A.; Schaefer, W. P.; Serfas, M.; Bercaw, J. E. *Organometallics* **1987**, *6*, 1219.
(17) Shapley, J. R.; Calvert, R. B. *J. Am. Chem. Soc.* **1978**, *100*, 7726.
(18) Coffindaffer, T. W.; Rothwell, I. P.; Huffman, J. C. *J. Chem. Soc., Chem. Commun.* **1983**, 1249.
(19) Chisholm, M. H.; Eichhorn, B. W.; Folting, K.; Huffman, J. C.; Tatz, R. J. *Organometallics* **1986**, *5*, 1599.

$Pr)_4$ (3), analogues of the structurally characterized compound $(t\text{-BuO})_2(W(\mu\text{-}C_2Ph_2)_2W(O\text{-}t\text{-Bu})_2$.[20]

## Experimental Section

**General Procedures.** See ref 1 for details.

**Chemicals.** The compounds **1a**, **1b**, **1c**,[1] and $W_2(CH_2\text{-}t\text{-}Bu)_2(O\text{-}i\text{-}Pr)_4$[19] were prepared by published methods. Synthesis of the deuteriated benzyl complexes (**1a**)(Ph-$d_7$) and (**1c**)(Ph-$d_7$) are reported herein. Ethyne, 2-butyne, and 2-pentyne were purchased commercially. *i*-PrOD was made from LiO-*i*-Pr and $D_2O$.

**Kinetics.** The rate studies were monitored by $^1H$ NMR spectroscopy using a Nicolet NT-360 spectrometer equipped with a variable-temperature probe and an automated kinetics software package (KINET). The solutions of **1a** and **1c** were prepared in a drybox by using dry and deoxygenated benzene-$d_6$ solvent and Pyrex NMR tubes with glass extensions. The sample concentrations were typically 0.03 M but were not rigorously measured after the reactions were determined to be first-order. The solutions were frozen at −198 °C and evacuated and the NMR tubes sealed with a torch. With the exception of $W_2(CH_2SiMe_3)_2(MeCCMe)_2(O\text{-}i\text{-}Pr)_4$, all reactions were conducted in a thermostated GC oven (±1 °C) in the dark. The temperatures ranged between 60 and 85 °C. The samples were periodically removed from the oven, quickly cooled (frozen) to 0 °C in an ice–water bath, and warmed to room temperature for NMR spectroscopic analysis. During sample preparation and NMR spectroscopic monitoring, no significant (detectable) reaction occurred. The decompositions of $W_2(CH_2SiMe_3)_2(MeCCMe)_2(O\text{-}i\text{-}Pr)_4$ were monitored in an NMR probe that was preheated to a desired temperature. The probe temperatures were calibrated by using an external ethylene glycol standard. All reactions were followed by monitoring the disappearance of compounds **1a** or **1c** using absolute-intensity integrations. Each reaction was monitored for no less than 2.5 half-lives and, in most cases, up to 4.0 half-lives. Each experiment was run twice, and the average rate constant ($k$) for a given reaction is reported in Table X. The rate constants and Eyring parameters were calculated by standard least-squares plots using a computer package written by Professor J. G. Gajewski. The reported errors in the rate constants were derived from the upper and lower limits of the least-squares deviations of the two runs for each experiment. The errors for the activation parameters are the least-squares standard deviations.

Spin–lattice relaxation times ($T_1$) were measured in an oxygen-free benzene-$d_6$ solution by using a standard spin inversion/recovery program on a Nicolet NT-360 NMR spectrometer.

The NOE difference experiments were run on a Nicolet NT-360 NMR spectrometer using a standard presaturation (PRESAT) program. Four-second presaturations (35-dB decoupling power) and 200-$\mu$s mixing times were employed. An interacquisition delay of 13 s was used which is more than 5 times larger than the longest $T_1$ (see Table VIII). Four concurrent experiments were run in which the decoupler frequency was set at 5.39, 8.56, 20.35, and 30 ppm corresponding to the O-*i*-Pr methine, CPh ortho hydrogen, and hydride resonances, and a background spectrum, respectively. The four data sets were collected concurrently to average any temperature change or field drift. The large differences in chemical shifts between the hydride resonance and any other resonance (>11 ppm) allowed for total presaturation and subsequent calculations of percent enhancements without using a DANTE pulse sequence.

**$H_2$ Analysis.** The molecular hydrogen byproduct was analyzed by mass spectroscopy through the courtesy of Christopher Hoham and Professor John M. Hayes. A weak $H_2$ signal was observed from a thermolyzed solid-state sample of (**1a**)($SiMe_3$) sealed under vacuum. The signal intensity was less than was anticipated for the sample size.

**Product Partitioning Experiments Involving the Conversion of (1a)($SiMe_3$) to (2)H($SiMe_3$) and (2)R($SiMe_3$).** Table XI lists 15 experiments that were carried out concurrently in a drybox over a 48-h period. Each experiment involved 8 mg of (**1a**)($SiMe_3$) and 600 $\mu$L of dry and deoxygenated solvent in the reaction vessel specified in the table. Normal glassware preparation, denoted by "N" in Table XI, involved (a) soaking the reaction vessel in a saturated KOH/EtOH bath for 24 h, (b) rinsing with copious amounts of $H_2O$, (c) rinsing with 3 N $HNO_3$, (d) rinsing with copious amounts of $H_2O$, (e) rinsing with EtOH (95%), and (f) heating in a drying oven (130 °C) for greater than 5 h. Acid washing, denoted by "A" in Table XI, proceeded in a similar fashion except the vessel was soaked in 3 N $HNO_3$ for 12 h at step c. Base washing, denoted by "B" in Table XI, was also identical with type "N" preparation except step c was not performed. New, previously unused reaction vessels, denoted by "V" in Table XI, were rinsed with EtOH and heated in a drying oven (130 °C) for greater than 5 h. Teflon-coated stir bars were soaked in concentrated $HNO_3$ for greater than 1 day, rinsed with copious amounts of $H_2O$, rinsed with EtOH, and heated in a drying oven (130 °C) for greater than 1 day prior to use.

**Table XI. Product Partitioning Results from Thermolyses of $W_2(CH_2SiMe_3)_2(MeCCMe)_2(O\text{-}i\text{-}Pr)_4$[a]**

| sample run | vessel type[b] | glassware preparation[c] | solv[d] | stir bar[c] | (2)H($SiMe_3$):(2)-R($SiMe_3$) ratio[e] |
|---|---|---|---|---|---|
| 1 | NMR | V | $C_6D_6$ | n | 90:10 |
| 2 | NMR | N | pentane | n | 88:12 |
| 3 | NMR[f] | N | $C_6D_6$ | n | 66:34 |
| 4 | NMR | V | $C_6D_6$ | y | 91:9 |
| 5 | NMR | A | $C_6D_6$ | n | 91:9 |
| 6 | NMR | B | $C_6D_6$ | n | 92:8 |
| 7 | vial | V | $C_6D_6$ | y | 67:33 |
| 8 | vial | V | $C_6D_6$ | n | 57:43 |
| 9 | vial | A | $C_6D_6$ | n | 58:42 |
| 10 | vial | B | $C_6D_6$ | n | 57:43 |
| 11 | vial[f] | V | $C_6D_6$ | n | 52:48 |
| 12 | vial[g] | V | $C_6D_6$ | n | 47:53 |
| 12 | Schlenk | N | $C_6D_6$ | y | 52:48 |
| 14 | Schlenk | N | $C_6D_6$ | n | 45:55 |
| 15 | Schlenk | B | $C_6D_6$ | n | 45:55 |

[a] See Experimental Section for procedural details. [b] NMR denotes a Pyrex NMR tube (5 mm); vial denotes a 10-mL snap-cap storage vial; Schlenk denotes a standard 40-mL Schlenk flask. [c] Abbreviations: N, normal; A, acid wash; B, base wash; V, new vessel; y, yes; n, no. See Experimental Section for details. [d] 600 $\mu$L of dry, deoxygenated solvent. [e] As determined by $^1H$ NMR spectroscopic integrations. [f] Vessel was charged with finely ground Pyrex glass (ca. 1 g) prior to reaction. [g] Vessel was charged with finely ground NMR tube glass (ca. 0.5 g) prior to reaction.

The relative product concentrations were determined by $^1H$ NMR spectroscopy by comparing the integral intensities of the $W_2(\mu\text{-}C_4Me_4)$ methyl singlets of (2)H($SiMe_3$) and (2)R($SiMe_3$) at 2.15 and 1.76 ppm, respectively. Samples 1 and 2 (Table XI) were transferred to separate weighing pans after the 48-h thermolysis period, and their solvents allowed to evaporate. The entire residues were then extracted into $C_6D_6$ (600 $\mu$L) and transferred to new NMR tubes. Sample 3 was filtered through glass wool into a clean NMR tube after thermolysis. The stir bar was removed from sample 4 after thermolysis but prior to NMR spectroscopic analysis. Samples 11 and 12 were filtered through glass wool directly into NMR tubes after thermolysis. All other samples were transferred directly into NMR tubes following thermolysis.

Three other experiments were conducted that are not listed in Table XI.

(1) **Light and Benzophenone.** Two separate Schlenk reaction vessels were charged with ca. 10 mg of (**1a**)($SiMe_3$) each. One flask was charged with pentane (10 mL) that was distilled from Na/benzophenone and stored under $N_2$ over 4-Å molecular sieves. The other flask was charged with spectrograde pentane (10 mL) that was degassed and dried over 4-Å molecular sieves but not distilled. The latter reaction vessel was covered with aluminum foil to exclude light. The solutions were magnetically stirred for 48 h at room temperature and then evaporated to dryness. The *entire* residues of each flask were extracted into $C_6D_6$ (ca. 500 $\mu$L) and analyzed by $^1H$ NMR spectroscopy. The product ratios were ca. 50:50 in each case.

(2) ***i*-PrOH.** A Pyrex NMR tube with a glass extension was charged with (**1a**)($SiMe_3$), $C_6D_6$ (500 $\mu$L), and *i*-PrOH (ca. 5 $\mu$L).

(20) Cotton, F. A.; Schwotzer, W.; Shamshoum, E. S. *Organometallics* **1983**, *2*, 1167.

The solution was then frozen at −198 °C and the tube evacuated and sealed with a torch. After 1 week at room temperature, a ca. 90:10 ratio of (2)H($SiMe_3$) to (2)R($SiMe_3$) was observed by $^1H$ NMR spectroscopy. No decomposition products were observed.

**(3) $C_6H_6$ vs $C_6D_6$.** An experiment similar to that described for (1) was followed except with $C_6H_6$ (distilled from Na/benzophenone) and $C_6D_6$ (not distilled). Both were left open to light. $^1H$ NMR spectroscopic analysis indicated a ca. 50:50 ratio of (2)H($SiMe_3$) to (2)R($SiMe_3$) in both cases.

**$HW_2(\mu\text{-C-}t\text{-Bu})(\mu\text{-}C_4Me_4)(O\text{-}i\text{-Pr})_4$.** In a Schlenk reaction vessel, $W_2(CH_2\text{-}t\text{-Bu})_2(O\text{-}i\text{-Pr})_4$ (509 mg, 0.683 mmol) was dissolved in hexane (20 mL). The orange solution was frozen at −198 °C, and 2-butyne (2 equiv, 1.37 mmol) was condensed into the flask by using a calibrated vacuum manifold. The frozen mixture was rapidly warmed to room temperature during which time the color changed from orange to dark green and slowly faded to brown after ca. 10 min. After the solution was stirred for 12 h at room temperature, the solvent was removed in vacuo, the brown solid was extracted into pentane (ca. 3 mL), and the solution cooled to −78 °C for 48 h. A brown, noncrystalline solid was collected by filtration and dried in vacuo (yield 120 mg, 23%). All attempts to crystallize the compound in a variety of solvents proved unsuccessful; however, sublimation of the crude brown reaction mixture (80 °C ($10^{-3}$ Torr)) afforded a lower yield (ca. 10%) of a higher purity product (noncrystalline). No other products could be detected by $^1H$ NMR. Anal. Calcd for $W_2O_4C_{25}H_{50}$ (brown sublimate). (Correct empirical formula with mol wt 950.08): C, *38.4*; H, 6.4; N, 0.0. Found: C, *37.0*; H, 6.1; N < 0.03. Calcd for $W_2O_4C_{24}H_{50}$ (but with mol wt 950.08): C, *36.9*; H, 6.4; N, 0.0.

IR data (Nujol mull between CsI plates, $cm^{-1}$): 1910 (m, br), 1582 (vw), 1365 (s), 1320 (m), 1260 (w), 1227 (w), 1165 (m), 1115 (s), 1017 (m), 979 (s), 851 (m), 800 (w), 737 (vw), 720 (vw), 695 (vw), 634 (w), 617 (m), 597 (vw), 461 (w), 299 (w).

**$HW_2(\mu\text{-CPh})(\mu\text{-}C_4Me_4)(O\text{-}i\text{-Pr})_4$.** In a Schlenk reaction vessel fitted with a reflux condenser, $W_2(CH_2Ph)_2(MeCCMe)_2(O\text{-}i\text{-Pr})_4$ (330 mg, 0.37 mmol) was dissolved in hexane (15 mL). The solution was refluxed for 24 h. The orange-brown solution slowly faded to a lighter brown color as the reaction proceeded. Following reflux, the solution was evaporated to dryness and the residue extracted into pentane (ca. 2 mL) and cooled to −20 °C for 12 h. Small orange-brown crystals were harvested by removing the supernatant liquid via cannula and drying in vacuo (crystalline yield 55 mg, 19%).

IR data (Nujol mull between CsI plates, $cm^{-1}$): 1870 (m), 1580 (w), 1478 (m), 1360 (s), 1322 (m), 1318 (m), 1257 (vw), 1161 (m), 1110 (vs), 1015 (s), 1001 (s), 969 (s), 960 (s), 849 (m), 760 (m), 689 (m), 638 (vw), 608 (m), 598 (m), 588 (m), 571 (m), 524 (w), 491 (vw), 459 (w), 428 (w).

Anal. Calcd for $W_2O_4C_{27}H_{46}$ (correct empirical formula with mol wt 802.4): C, *40.4*; H, 5.7; N, 0.0. Found: C, *39.3*; H, 5.2; N, <0.03. Calcd for $W_2O_4C_{26}H_{46}$ (but with mol wt 802.4): C, *38.9*; H, 5.7; N, 0.0.

**$HW_2(\mu\text{-CSiMe}_3)(\mu\text{-}C_4Me_4)(O\text{-}i\text{-Pr})_4$.** In a Schlenk reaction vessel, $W_2(CH_2SiMe_3)_2(O\text{-}i\text{-Pr})_4$ (584 mg, 0.75 mmol) was dissolved in hexane (20 mL) and frozen at −198 °C. 2-Butyne (2.05 equiv, 1.54 mmol) was condensed onto the frozen solution by using a calibrated vacuum manifold. The mixture was rapidly warmed to room temperature and stirred under $N_2$ for 24 h. The color rapidly changed from orange-brown to burnt orange upon warming and then slowly faded to brown over the 24-h period. The solvent was then removed in vacuo and the reaction flask fitted with a water-cooled cold finger and heated to 70 °C at $10^{-3}$ Torr. The product sublimed slowly over a 2-day period yielding a yellow-brown noncrystalline solid (yield 283 mg, 51%).

IR data (KBr pellet, $cm^{-1}$): 2968 (vs), 2925 (s), 2882 (s), 1858 (m, br), 1580 (vw), 1460 (m), 1444 (m), 1398 (w), 1378 (s), 1361 (s), 1326 (m), 1314 (m), 1241 (s), 1163 (s), 1119 (vs), 1018 (vs), 1000 (vs), 976 (vs), 968 (vs), 840 (vs), 751 (m), 688 (w), 635 (w), 611 (m), 589 (m), 528 (w), 462 (w), 338 (w).

Anal. Calcd for $W_2O_4SiC_{24}H_{50}$ (correct empirical formula with mol wt 798.14): C, *36.1*; H, 6.3. Found: C, *34.7*; H, 5.9. Calcd for $W_2O_4SiC_{23}H_{50}$ (but with mol wt 798.14): C, *34.6*; H, 6.3.

**$(Me_3SiCH_2)W_2(\mu\text{-CSiMe}_3)(\mu\text{-}C_4Me_4)(O\text{-}i\text{-Pr})_4$.** In a Schlenk reaction vessel, $W_2(CH_2SiMe_3)_2(O\text{-}i\text{-Pr})_4$ (544 mg, 0.70 mmol) was dissolved in hexane (15 mL) and frozen at −198 °C. With use of a calibrated vacuum manifold, 2-butyne (2.2 equiv, 1.54 mmol) was condensed onto the frozen mixture. The flask was quickly warmed to room temperature and stirred for 4 days. The color rapidly turned from orange brown to burnt orange upon warming and then slowly faded to yellow brown over a 24-h period. After 4 days, the solution was filtered through a fine frit, evaporated to dryness in vacuo, and extracted into THF (ca. 5 mL). The yellow-brown mixture was concentrated to ca. 2 mL and cooled to −20 °C. After 5 days, 156 mg of pale orange crystalline material was isolated by removing the supernatant liquid via cannula. The isolated sample contained ca. 10% $HW_2(\mu\text{-CSiMe}_3)(\mu\text{-}C_4Me_4)(O\text{-}i\text{-Pr})_4$ impurity as determined by $^1H$ NMR spectroscopy. The crystalline material was redissolved in dimethoxyethane (3 mL) at 50 °C. The orange-yellow solution was allowed to slowly cool to room temperature over a 2 h period. After 2 days at room temperature, 66 mg of spectroscopically pure pale orange crystals was isolated by removing the solvent via cannula and drying in vacuo (crystalline yield 66 mg, 11.5%). Crystals grown in this way were used in the X-ray study.

IR data (KBr pellet, $cm^{-1}$): 2975 (vs), 2925 (s), 2893 (s), 2628 (vw), 1460 (m), 1400 (w), 1378 (s), 1359 (m), 1330 (m), 1322 (m), 1258 (m), 1242 (s), 1162 (s), 1120 (vs), 1010 (vs), 985 (vs), 922 (w), 909 (m), 840 (vs), 785 (w), 750 (m), 729 (w), 682 (w), 648 (m), 632 (m), 621 (m), 580 (m), 458 (vw), 332 (m).

**$W_2(CH_2\text{-}t\text{-Bu})_2(O\text{-}i\text{-Pr})_4$ + Excess MeC≡CEt.** In a Schlenk reaction vessel, $W_2(CH_2\text{-}t\text{-Bu})_2(O\text{-}i\text{-Pr})_4$ (70 mg, 0.09 mmol) was dissolved in hexane (10 mL) producing an orange-brown solution. With the use of a microsyringe, MeC≡CEt (19 μL, 0.19 mmol, 2.1 equiv) was added to the solution at room temperature resulting in a color change from orange to brown after ca. 5 s. The mixture was stirred for an additional 1 h and was then evaporated to dryness under dynamic vacuum. An aliquot of the resulting brown oil was analyzed by $^1H$ NMR spectroscopy. The Schlenk flask with the remaining oily residue was fitted with a water-cooled cold finger and heated to 70 °C under dynamic vacuum ($10^{-3}$ Torr) for 12 h. The resulting brown oil that deposited on the cold finger was analyzed by $^1H$ NMR spectroscopy. The two oils were spectroscopically identical.

**$W_2(CD_2C_6D_5)_2(R'CCR')_2(O\text{-}i\text{-Pr})_4$ Where R′ = Me or Et.** The deuteriated compounds were prepared from 1,2-$W_2(CD_2C_6D_5)_2(O\text{-}i\text{-Pr})_4$ and R′C≡CR′ (where R′ = Me or Et) employing the same reaction conditions described for the protio analogues.[1] 1,2-$W_2(CD_2C_6D_5)_2(O\text{-}i\text{-Pr})_4$ was prepared from 1,2-$W_2(CD_2C_6D_5)_2(NMe_2)_4$ and *i*-PrOH by using the general procedures previously described.[19] 1,2-$W_2(CD_2C_6D_5)_2(NMe_2)_4$ was synthesized from Li($CD_2C_6D_5$)·TMEDA and 1,2-$W_2Cl_2(NMe_2)_4$ in a manner similar to previously published methods.[21] Li($CD_2C_6D_5$)·TMEDA was prepared from toluene-$d_8$ by using *n*-BuLi in the presence of 1.0 equiv of TMEDA.

**Photolysis of Compounds 1a and 1c.** A typical experiment involved 0.02 mmol of compound dissolved in 0.6 mL of $C_6D_6$ in an extended Pyrex NMR tube. The samples were then frozen at −198 °C, evacuated, and sealed with a torch. The solutions were then photolyzed in a water-cooled bath (10 °C) by using a 550-W Hanovia photolysis lamp. The reactions were monitored periodically by $^1H$ NMR spectroscopy. When noted, 1,4-cyclohexadiene was added via a syringe to the $C_6D_6$ solutions.

**$HW_2(\mu\text{-CPh})(\mu\text{-}C_4Me_4)(O\text{-}i\text{-Pr})_4$ + $H_2$ (500 psi).** In the Pyrex insert of a high-pressure reaction vessel, $HW_2(\mu\text{-CPh})(\mu\text{-}C_4Me_4)(O\text{-}i\text{-Pr})_4$ (20 mg, 0.025 mmol) was dissolved in hexane (5 mL) in a drybox. The reaction vessel was then sealed, charged with 500 psi of $H_2$, and the solution was stirred for 24 h at room temperature. The $H_2$ gas was then released and the solution transferred to a Schlenk flask in the drybox. The hexane was removed under dynamic vacuum and the resulting orange-brown residue extracted into $C_6D_6$ (0.5 mL). $^1H$ NMR spectroscopic analysis revealed only $HW_2(\mu\text{-CPh})(\mu\text{-}C_4Me_4)(O\text{-}i\text{-Pr})_4$.

**$(Me_3SiCH_2)W_2(\mu\text{-CSiMe}_3)(\mu\text{-}C_4Me_4)(O\text{-}i\text{-Pr})_4$ + $H_2$.** In a Pyrex NMR tube with a glass extension, $(Me_3SiCH_2)W_2(\mu\text{-CSiMe}_3)(\mu\text{-}C_4Me_4)(O\text{-}i\text{-Pr})_4$ (15 mg) was dissolved in $C_6D_6$ (0.5 mL) and the solution frozen at −198 °C. The NMR tube was charged to greater than 1 atm of $H_2$ by submerging the NMR tube into liquid $N_2$, evacuating the gasses, and then opening the tube

(21) Chetcuti, M. J.; Chisholm, M. H.; Folting, K.; Haitko, D. A.; Huffman, J. C.; Janos, J. *J. Am. Chem. Soc.* **1983**, *105*, 1163.

to a calibrated vacuum manifold charged with 1 atm of $H_2$. The NMR tube was then sealed with a torch. Subsequently, $^1H$ NMR spectra were recorded periodically over a 2-day period. No apparent reaction was observed.

**$HW_2(\mu\text{-}CR)(\mu\text{-}C_4Me_4)(O\text{-}i\text{-}Pr)_4$ + Acetylenes.** Typical experiments involved 20 mg of (2)H dissolved in hexane (~5 mL) in a Schlenk flask. The solutions were frozen at −198 °C and acetylene (≫2 equiv) condensed into the flask. The frozen mixtures were rapidly warmed to 0 °C in an ice–water bath and allowed to stir at room temperature for ca. 1 h. In most cases, copious amounts of precipitate (polyacetylene) formed after ca. 5 min. The solutions were then evaporated to dryness under dynamic vacuum and the benzene-soluble residues extracted into $C_6D_6$ (ca. 0.5 mL). $^1H$ NMR analysis of the orange-brown $C_6D_6$ solutions revealed only (2)H.

**$HW_2(\mu\text{-}CSiMe_3)(\mu\text{-}C_4Me_4)(O\text{-}i\text{-}Pr)_4$ + Excess $SiMe_4$.** In a Pyrex NMR tube with a glass extension, $HW_2(\mu\text{-}CSiMe_3)(\mu\text{-}C_4Me_4)(O\text{-}i\text{-}Pr)_4$ (ca. 10 mg) was dissolved in $C_6D_6$ (0.5 mL). A large excess of $SiMe_4$ (ca. 100 μL) was added to the solution via microliter syringe. The mixture was then frozen at −198 °C and evacuated and the NMR tube sealed with a torch. Periodic analysis by $^1H$ NMR spectroscopy revealed no reaction even after 1 week.

**$HW_2(\mu\text{-}CR)(\mu\text{-}C_4Me_4)(O\text{-}i\text{-}Pr)_4$ + *i*-PrOD or LiO-*i*-Pr.** Typical experiments involved mixing equimolar quantities of (2)H with *i*-PrOD or LiO-*i*-Pr (or both) in $C_6D_6$ solvent (0.5 mL) in Pyrex NMR tubes. The reactions were monitored by $^1H$ NMR spectroscopy. The hydride resonances were not affected in any experiment.

**Crystallographic Studies.** General operating procedures and listings of programs have been previously given.[22]

**$W_2(H)(\mu\text{-}CPh)(\mu\text{-}C_4Me_4)(O\text{-}i\text{-}Pr)_4$.** A small well-formed crystal was transferred to the goniostat where it was cooled to −159 °C for characterization and data collection. A systematic search of a limited hemisphere of reciprocal space located a set of diffraction maxima which were of orthorhombic symmetry and with axial extinctions corresponding to space group $P2_12_12_1$.

Data were collected for $+h,+k,+l$ and reduced in the usual manner, correcting for Lorentz and polarization as well as absorption. The structure was solved by direct methods (MULTAN78) and Fourier techniques. Many of the hydrogen positions could be located in a difference Fourier phased on the non-hydrogen parameters, and all but the four methyl groups on the "flyover" were given idealized fixed hydrogen coordinates for the final cycles. Unfortunately, the hydride was not visible. The coordinates reported are for the correct enantimorph for the crystal studies, based on refinement of both choices. A final difference Fourier was featureless, the largest peak being 0.35 e/Å$^3$.

**$W_2(CH_2SiMe_3)(\mu\text{-}CSiMe_3)(\mu\text{-}C_4Me_4)(O\text{-}i\text{-}Pr)_4$.** A suitable crystal was located and transferred to the goniostat by using inert-atmosphere handling techniques and cooled to −155 °C for characterization and data collection. A systematic search of a limited hemisphere of reciprocal space failed to locate any systematic absences or symmetry indicating a triclinic space group. Subsequent solution and refinement of the structure confirmed the centrosymmetric $P\bar{1}$ choice.

Data were collected in the usual manner by using a continuous $\theta$–$2\theta$ scan with fixed backgrounds. Data were reduced to a unique set of intensities and associated $\sigma$'s in the usual manner. Due to the fact that the crystal was poorly defined and relatively small, no absorption correction was performed. A $\psi$ scan of two reflections indicated absorption was not a problem.

The structure was solved by a combination of direct methods (MULTAN78) and Fourier techniques, and the heavy-atom positions confirmed by a Patterson synthesis. The positions of all hydrogen atoms were clearly visible in a difference Fourier phased on the non-hydrogen atoms, and the coordinates and isotropic thermal parameters for hydrogens were varied in the final cycles of refinement.

A final difference Fourier was essentially featureless, with the largest peak being 1.3 e/Å$^3$ located adjacent to W(1).

**Acknowledgment.** We thank the National Science Foundation for support. B.W.E. was the 1985–1987 Indiana University SOHIO graduate fellow.

**Registry No.** (**1a**) ($SiMe_3$), 116563-27-0; (**1a**) (Ph), 99639-37-9; (**1a**) (*t*-Bu), 116699-48-0; (**2**)H($SiMe_3$), 116699-57-1; (**2**)-$Me_3SiCH_2(SiMe_3)$, 116699-54-8; (**2**)H(*t*-Bu), 116699-55-9; (**2**)H(Ph), 116699-56-0; $W_2(CH_2\text{-}t\text{-}Bu)_2(O\text{-}i\text{-}Pr)_4$, 101860-13-3; MeC≡CMe, 503-17-3; $W_2(CH_2SiMe_3)_2(O\text{-}i\text{-}Pr)_4$, 116563-40-7; MeC≡CEt, 627-21-4; $W_2(CD_2C_6D_5)_2(MeCCMe)_2(O\text{-}i\text{-}Pr)_4$, 116699-49-1; $W_2$-$(CD_2C_6D_5)_2(EtCCEt)_2(O\text{-}i\text{-}Pr)_4$, 116699-50-4; 1,2-$W_2(CD_2C_6D_5)_2$-$(O\text{-}i\text{-}Pr)_4$, 116699-52-6; EtC≡CEt, 928-49-4; 1,2-$W_2(CD_2C_6D_5)_2$-$(NMe_2)_4$, 116699-53-7; $Li(CD_2C_6D_5)$·TMEDA, 116699-51-5; 1,2-$W_2Cl_2(NMe_2)_4$, 63301-81-5; toluene-$d_8$, 2037-26-5.

**Supplementary Material Available:** Tables of anisotropic thermal parameters and complete listings of bond distances and angles and stereoviews (14 pages); listings of $F_o$ and $F_c$ values (20 pages). Ordering information is given on any current masthead page.

(22) Chisholm, M. H.; Folting, K.; Huffman, J. C.; Kirkpatric, C. C. *Inorg. Chem.* **1984**, *23*, 1021.